It is only when they go wrong that machines
remind you how powerful they are.
- Clive James.

CHAPTER 4

STRUCTURAL TECHNIQUES

In chapter 2 we noted in advance that the structures of glasses and other amorphous materials are quite complex. The absence of 3-dimensional periodicity takes away the convenience of describing the structure in terms of a few parameters like inter atomic distances, bond angles and symmetry which describe the unit cell. Therefore the description of the glass structure with the same precision as that of a crystal is impossible. We may easily visualize that every chosen arbitrarily small part of a glass is in principle structurally different from the other. It is as if glass is an assembly of an infinitely large number of polyamorphic phases with no discernable differences in their thermodynamic properties. This also introduces a new dimension to the problem because the history of preparation itself can introduce different structures. Therefore we are restricted to discuss the structure in terms of an averaged 1-dimensional description of amorphous solids through their radial distribution functions (RDF). It is one dimensional because glasses are isotropic in their structure and properties. The RDF to be discussed further below describes how the number densities of atoms vary as a function of distances from an arbitrarily chosen atom at the centre. Although various notations have been used for RDF in the literature, we use here the more familiar notation of $G(r)$ and define RDF. $G(r)$ is defined in terms of the function $\rho(r)$ as

$$G(r) = 4\pi r^2 \rho(r) \tag{4.01}$$

where $\rho(r)$ gives the number of atoms lying between r and $(r + dr)$ from a given atom as shown in Figure 4.01 (a). $\rho(r)$ is the radial density function. $\rho(r)$ and $G(r)$ are shown in Figure 4.01b and 4.01c respectively. Pair correlation function is evidently zero at values of r less than the average nearest neighbour distance since there are no atoms in that range. $\rho(r)$ itself should acquire a constant average value which is ρ^0 for large values of r as shown by the dotted line in Figure 4.01b. Similarly in the RDF shown in Figure 4.01 (c), the dotted line represents $4\pi r^2\rho^0$ line. The undulations around the dotted line mark the distances at which the number

density increases. This is because from the chosen arbitrarily center these are the distances at which other atoms are located. Before we proceed further, we take note of two other correlation functions generally used to represent data. They are the differential correlation function $D(r)$, given by

$$D(r)=4\pi r[\rho(r)-\rho^0] \tag{4.02}$$

and the total correlation function $T(r)$, given by

$$T(r) = 4\pi r\rho(r) \tag{4.03}$$

and they are shown in Figure 4.01(d) and 4.01(e) respectively. We will discuss how the RDFs are obtained from experiments little later. The structural investigations of a glass consists in understanding the origin of the few peaks seen in RDF.

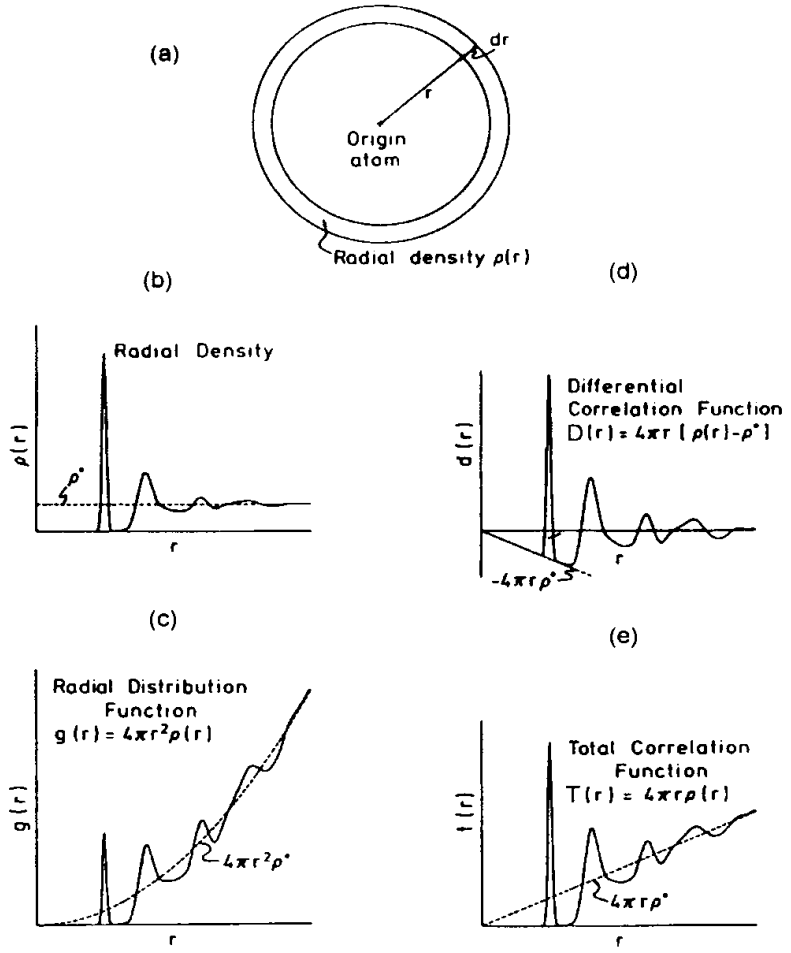

Figure 4.01: Real space correlation functions for a monatomic amorphous solid.

Consider the example of SiO_2 glass. We know for certain from chemical considerations that silicon should be present in $[SiO_{4/2}]^0$ tetrahedra in the glass structure. Figure 4.02 shows how the silicate tetrahedra are connected. It is the variation of the torsional and bond angles α and β which gives rise to a non-crystalline arrangement of the tetrahedra. We expect to be able to analyse RDF of SiO_2 and to provide the information of bond distances and the bond angles.

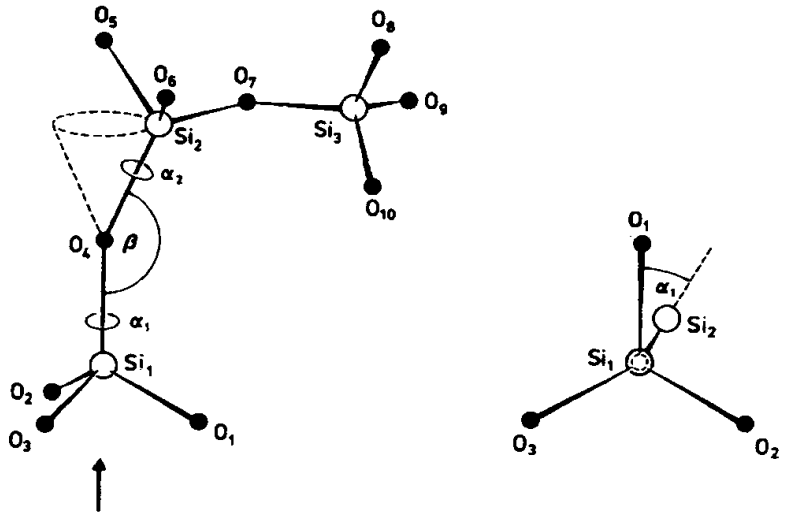

Figure 4.02: Definition of the bond angle, β and the torsion angle α_1 and α_2 for vitreous silica.

X-ray diffraction from glass

The diffraction experiment conducted with a glassy sample is no different from that with a crystalline material (Warren, 1969; Wright, 1974; Wright and Leadbetter, 1976; Wagner, 1978;). In a diffractometer, X-rays are incident on a sample surface at an angle θ to its normal and are diffracted at an angle 2θ with respect to the incident beam direction. Intensities of the diffracted beams are recorded as a function of 2θ. The scattering geometry and the relation between the scattering vectors are shown in Figure 4.03. If the scatterers are point charges, then the scattering intensity, I_{eu}, is given by,

$$I_{eu} = f_e f_e^* \tag{4.04}$$

Where f_e is the scattering factor, which is complex and is given by,

$$f_e = \int \exp[(2\pi i / \lambda)(\mathbf{s} - \mathbf{s}_0).\mathbf{r}]\rho(r)dV \qquad (4.05)$$

where the electron charge is assumed to be distributed in a small volume dV and $\rho(r)$ is the corresponding density variation as a function of r.

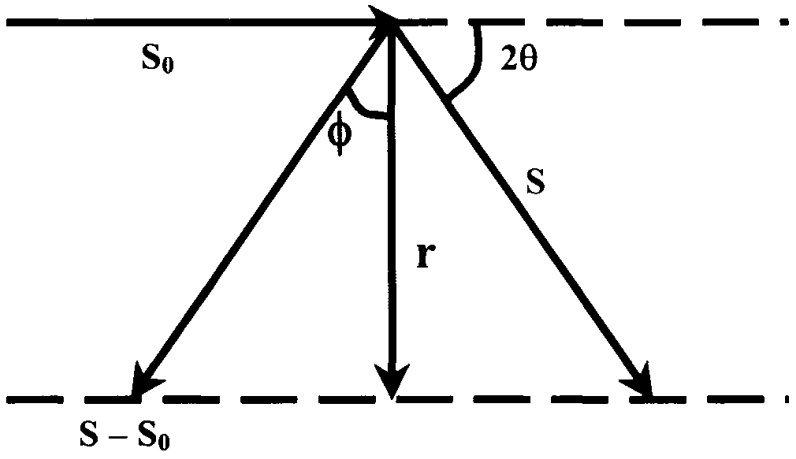

Figure 4.03: Relation between scattering vectors.

On the basis of Figure 4.03, the dot product $(\mathbf{s} - \mathbf{s}_0).\mathbf{r}$ is easily seen to be equal to $2r\sin\theta\cos\phi$. Substituting for λ from the relation $k = (4\pi\sin\theta)/\lambda$ in the exponential, the scattering factor can be written in terms of ϕ and r as,

$$f_e = \int_{r=0}^{\infty}\int_{\phi=0}^{\pi} \exp[ikr\cos\phi]\rho(r).2\pi r^2 dr.\sin(\phi)d\phi \qquad (4.06)$$

in which electron distribution is assumed to have a spherical symmetry so that r is simply treated as a scalar. Integration over ϕ gives,

$$f_e = \int_0^{\infty} 4\pi r^2 \rho(r)\left(\frac{\sin kr}{kr}\right)dr \qquad (4.07)$$

This can be generalized to an atom where there are several electrons so that it represents the atomic scattering factor, also called the "form factor" and is given by,

$$f = \sum_n f_{e,n} = \sum_n \int_0^{\infty} 4\pi r^2 \rho_n(r)\left(\frac{\sin kr}{kr}\right)dr \qquad (4.08)$$

where again $\rho_n(r)$ is the density distribution of electrons. It is evident that the quantity, $\sum_n \int_0^\infty 4\pi r^2 \rho_n(r) dr$, should give the total number of electrons in the atom or atomic number, Z and (sin kr)/(kr) tends to unity for small value of r, therefore f itself tends to Z as k tends to zero. The atomic scattering factor, f, therefore is a function of k and the variation of $f(k)$ as a function of k is shown in Figure 4.04.

Figure 4.04: Schematic illustration of the dependence of the X-ray atomic form factor on scattering vector.

f_e in the scattering intensity function, I_{eu}, ($= f_e f_e^*$), is now the sum of the scattered amplitudes resulting from each atom. The amorphous solid is isotropic and the probability of finding two atomic scatterers at a distance r_{mn} from a given atom is identical in all directions. This property can be utilized to show that the scattering intensity I_{eu} for an assembly of atomic scatterers is given by the Debye equation,

$$I_{eu} = \sum_m \sum_n f_m f_n \frac{\sin kr_{mn}}{kr_{mn}} \qquad (4.09)$$

Let us suppose that the assembly we are considering consists of only one type of atoms. Then I_{eu} can be written as,

$$I_{eu} = \sum_m f^2 + \sum_m \sum_{n \neq m} f^2 \frac{\sin kr_{mn}}{kr_{mn}} \qquad (4.10)$$

This equation allows us to introduce a density function $\rho_m(r_{mn})$ considering m as the atom at the origin so that the summation can be substituted by an integration and I_{eu} is written as,

$$I_{eu} = \sum_m f^2 + \sum_m f^2 \int \rho_m(r_{mn}) \frac{\sin kr_{mn}}{kr_{mn}} .dV_m \tag{4.11}$$

Now the scattering intensity is over the sample volume with an assumed spherical symmetry. Expressing the density as an appropriate isotropic function of r and taking into consideration that at sufficiently large distances ρ tends to ρ^0, which is the constant average density, it can be shown that the above equation becomes

$$I_{eu} = Nf^2 + Nf^2 \int_0^\infty 4\pi r^2 [\rho(r) - \rho^0] \frac{\sin kr}{kr} .dr \tag{4.12}$$

where all the quantities are now referenced to macroscopic dimensions consisting of N atomic scatterers. We recognize that $4\pi r^2\rho(r)$, which is the radial distribution function should be related to the scattering intensity through a Fourier transformation. In order to achieve this, a reduced scattering intensity function, $F(k)$, has to be defined as,

$$F(k) = k\left[\frac{(I_{eu}/N) - f^2}{f^2}\right] \tag{4.13}$$

Using equation (4.12),

$$F(k) = k \int_0^\infty 4\pi r^2 [\rho(r) - \rho^0] \frac{\sin kr}{kr} .dr \tag{4.14}$$

The differential or reduced radial distribution function, $D(r)$, is given by,

$$D(r) = 4\pi r[\rho(r) - \rho^0] = \frac{G(r)}{r} - 4\pi r\rho^0 \tag{4.15}$$

These functions oscillate about zero and do not increase or decrease as functions of k or r. Therefore $F(k)$ itself is now equal to

$$F(k) = \int_0^\infty D(r).\sin kr.dr \tag{4.16}$$

Thus we have a function $F(k)$ which is obtained from the experimental scattering intensity in the k-space, which is related to pair distribution in the real space for an amorphous solid. They are therefore related through a Fourier transform which can be written as

$$D(r) = \frac{2}{\pi}\int_0^\infty F(k).\sin kr.dk \tag{4.17}$$

Although $\sin(kr)$ appears in both expressions, $\sin(kr)$ in k-space arises from the Debye equation, while in $D(r)$ it is a consequence of Fourier transform. How good is $D(r)$ depends on range of k, which is formally assumed to have a range of 0 to ∞, but in practice, it is limited by the energy of the X-ray photon.

The more useful RDF is therefore obtained starting from experimentally determined $F(k)$ but sometimes $F(k)$ itself can be used to examine subtle structural aspects. It may also be noted here that $F(k)$ is related to the structure factor $S(k)$, where $S(k)$ is defined as,

$$S(k) = \frac{I_{eu}(k)}{Nf^2} \tag{4.18}$$

so that $F(k) = k[S(k) - 1]$. The k-weighting of $S(k)$ in the expression for $F(k)$ makes it particularly useful in the high k range. It may also be noted that when $F(k)$ exhibits oscillatory behaviour up to very large values of k, it is indicative of the presence of well defined first coordination polyhedra in the structure and well defined first neighbour distances because the sinusoidals in the k-space are built by the Fourier transform (FT) of each and every peak in $D(r)$. The peaks in $D(r)$ correspond to successive coordination shells and quite generally exhibit increasing widths. Such wide peaks give rise to highly damped sinusoidal waves in Fourier transform. The only oscillations, which survive at large k values are those arising from the FT of the first peak in $D(r)$.

The use of X-ray diffraction technique to obtain structural information in glasses consist of collecting the total scattered intensity as a function of k. The collected intensity should be first corrected for incoherent contributions such as Compton scattering and any other background contributions. These intensities as expected oscillate around f^2 curve (see equation 4.12) from which $F(k)$ is computed as a function of k. Since f^2 decreases sharply as a function of θ, one would expect a sharp fall

off in intensity as a function of θ in XRD. The experimental set up is generally the same as that used for the study of the crystals. The diffraction of a collimated beam of X-rays is studied either in transmission or in reflection modes. In the laboratory, one uses either Mo Kα with λ = 0.71 Å or Cu Kα with λ = 1.54 Å. This limitation is overcome in synchrotron sources, where higher energies are available. X-ray energies are monochromatized by reflecting them off from a select plane of a single crystal (such as Si(111)) before collimation. The usual detector systems these days are solid state counters which give accurate measurements of X-ray intensities. The intensities are first corrected for contributions from the substrate, from the instrumental noise and from the polarization factor followed by a correction for Compton scattering. The corrected $I(k)$ is then converted into $F(k)$. The k-range is dependent on λ and the maximum values are 17.7 Å^{-1} for Mo Kα and just 8.2 Å^{-1} for Cu Kα. The Fourier transform of the data to obtain $D(r)$ assumes that we have infinite range of k values. Therefore this gives rise to what is known as termination error, because of the finite range of k. Termination error is reduced significantly in synchrotron work. λ can be taken down to ~ 0.1 Å. But in practice termination errors are reduced to a significantly low level by artificially smoothing the data around $k = k_{max}$ so that there is no discontinuity at k_{max}. One of these mathematical tricks is to Fourier transform $F(k).M(k)\sin(kr).dk$ instead of $F(k)\sin(kr).dk$, where $M(k)$ is $(k_{max}/\pi k).\sin(\pi k/k_{max})$ and is known as Lorch function (1969). Use of such functions generally reduces the real space resolution. It is worthwhile to note here that there are three important limitations of the XRD technique itself. The first is that the scattering intensity is superposed upon the f^2 function which is itself a function of k. This reduces the accuracy of intensity computed at high k values. Second is that the value of k_{max} attainable which is not sufficient with normal laboratory X-ray sources. The third point is that XRD in principle measures the electron density correlations, which for light atoms may not be the same as correlation of the atomic positions because significant fraction of electrons are in bonding (interatomic) regions.

Neutron scattering

Using neutron scattering (Wright, 1980) for structural work has several advantages. Most importantly, neutron sources from nuclear reactors have a wavelength range of 0.1-1 Å (corresponding to an energy range of 8 eV-80 meV). Secondly, the role of the atomic scattering factor,

f of XRD is replaced by the neutron scattering length, $\overline{b}$, which is isotropic and is independent of the value of k. The scattering is only by the nuclei. $\overline{b}$ values of isotopes of a given element can vary both in sign and magnitude. This is used to advantage in structural work because isotopic substitution can identify the source of observed scattering intensities. $\overline{b}$ is the average scattering length and its variation across the periodic table is shown in Figure 4.05. In neutron scattering therefore the atomic number of the scatterer is not a problem because light elements scatter as efficiently as heavier ones.

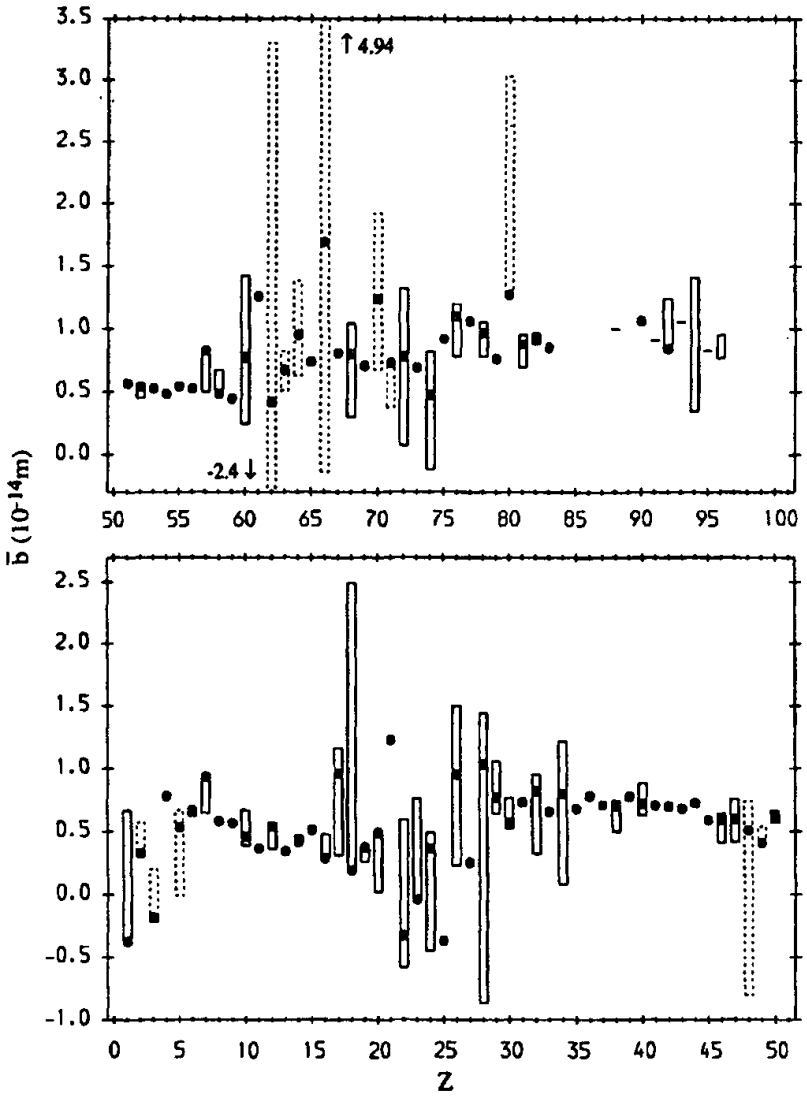

Figure 4.05: The neuron scattering length, $\overline{b}$, as a function of atomic number, Z, showing the value for the natural element ($\oplus$) and the range of isotopic variation (bar). A dashed bar denotes elements with complex $\overline{b}$ and only the variation in the real part of $\overline{b}$ at a wavelength of 1 Å (From Wright, 1993).

When a neutron beam is incident on a material, due to the large mass of neutron there is a great chance of energy and momentum transfer. This renders the inelastically (Compton) scattered component of neutrons quite significant. The inelastically scattered component contains dynamical information, which can be separated and analysed. Further, neutrons carry spins and therefore when the amorphous solid contain spin bearing species, there is a new contribution to the scattered intensity due to magnetic scattering which is also useful. However our focus in this section is confined to the elastic scattering of the neutrons from an amorphous solid from which structural information can be gathered. The scattering formalism is the same for both X-rays and neutrons. In the practice of neutron work, the scattering vector, k, is generally represented as Q. The scattering intensity is represented by the equation,

$$I_N^T(Q) = N\bar{b}^2 + N\bar{b}^2 \int_0^\infty 4\pi r^2 \rho(r) \frac{\sin Qr}{Qr} .dr \tag{4.19}$$

where the superscript, T and subscript, N on I indicate total (scattering) and neutron respectively. The expression for reduced intensity $F(k)$ is represented by,

$$F(k) = Q\,I(Q) \tag{4.20}$$

where $I(Q)$ is the equivalent of the reduced intensity in XRD. Therefore the working expression for structure work is,

$$QI_N(Q) = N\bar{b}^2 \int_0^\infty D(r) \sin Qr.dr \tag{4.21}$$

Use of the above expression is described as static approximation because all neutrons are detected irrespective of elastic or inelastic scattering. This is avoided by using an additional monochromator in a triple axes spectrometer in which only the elastically scattered neutrons are detected.

Inelastic neutron scattering

Inelastic neutron scattering (Sinclair, 1985; Leadbetter, 1973) can be used to investigate vibrational spectra of glasses. Thermalized neutrons have energies under 50 meV (roughly 400 cm^{-1}). Therefore, during the

process of neutron scattering, they interact with the particles in the glass to either loose part of their energy and create phonons or gain energy from phonons in the system. The process constitutes the inelastic neutron scattering. Therefore, in inelastic scattering, the scattering parameter becomes energy dependent. The structure factor is represented as $S(Q, \omega)$ rather than $S(Q)$. Therefore, the pair correlation function, which is the Fourier transform of $S(Q)$ would be a function of time, which is $G(r, t)$ instead of $G(r)$. $G(r, t)$ consists of self and distinct parts of the correlations, $G(r, t) = G_S(r, t) + G_D(r, t)$. At large values of Q, $G_D(r, t)$ can be neglected and this corresponds to the neglect of the contribution to the interference of neutrons scattered by other atoms. This is known as incoherent approximation and is valid for $Qr_0 >> 1$. Therefore retaining only the self-part amounts to scattering being proportional to the phonon density of states. It has been shown (Wright, 1980) that the density of states $\rho(\omega)$ can be obtained from scattering cross section as,

$$\rho(\omega) = cg(Q, \omega)$$

where

$$g(Q,\omega) = \left(\frac{d^2\sigma}{d\Omega dE'}\right).\frac{\mathbf{k}}{\mathbf{k}'}.\frac{2\omega}{N[n(\omega)+1]Q^2} \tag{4.22}$$

where the first term in the bracket is the neutron scattering cross section, $\mathbf{k}$ and $\mathbf{k}'$ are the incident and scattered wave vectors and $(n(\omega)+1)$ is the Boson factor, Q is the momentum transfer vector ($\hbar\mathbf{Q} = \hbar(\mathbf{k} - \mathbf{k}')$) and c is a frequency dependent term, given by,

$$c = \left[\frac{\langle\bar{b}^2\rangle}{M}\left(\langle u^2(\omega)\rangle e^{-2W}\right)\right] \tag{4.23}$$

$\langle\bar{b}^2\rangle$ is the average scattering length, M is the atomic mass, $\langle u(\omega)\rangle$ is the average displacement and e^{-2W} is the Debye-Waller factor.

Many glasses have been studied using inelastic neutron scattering. Vitreous SiO_2 has been investigated using inelastic neutron scattering and vibrational density of states has been obtained by Price and Carpenter (1987). The spectra are shown in Figure 4.06, which clearly reveals the existence of the splitting of the high frequency modes of SiO_2. One other interesting observation from inelastic neutron scattering studies has been

to show the absence of 808 cm^{-1} peak in B_2O_3 glass. The presence of this vibrational frequency has been ascertained in Raman studies. This observation led Elliott (1978) to consider that the contribution of boroxol rings may not be important to the structure of B_2O_3 (see chapter 12).

Electron scattering

Electrons are also used in scattering studies. An electron microscope is employed for the purpose in which the wavelength of the electrons is readily available down to 0.05 Å. The scattering of the electrons occurs both due to nuclei and electrons in the atoms. The scattering experiment consists of using constant λ and variable scattering angles by tilting the sample geometry. The term in electron diffraction corresponding to the atomic scattering factors in XRD is given by,

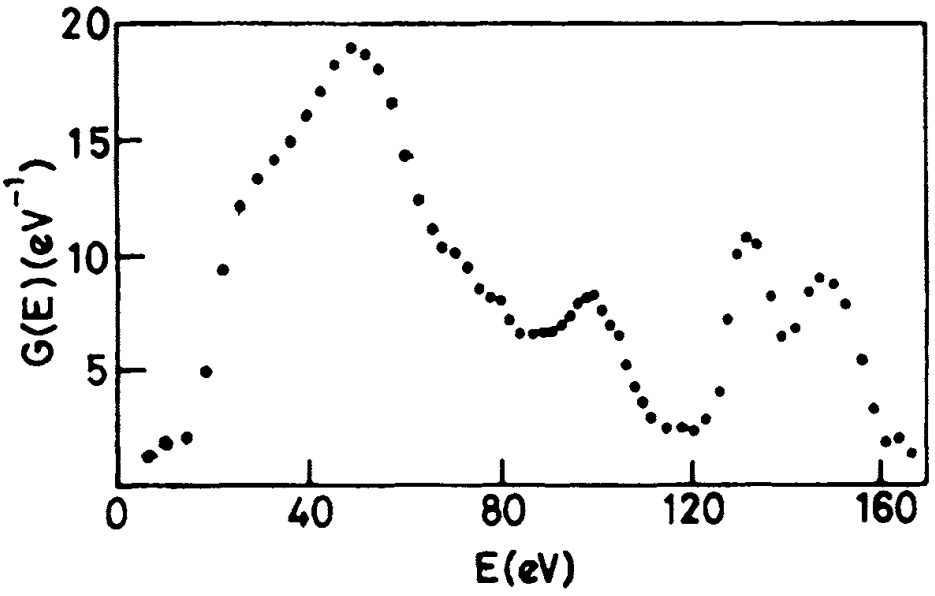

Figure 4.06: Effective density of states obtained from inelastic neutron scattering for vitreous silica (After Price and Carpenter, 1987).

$$f^e(k) = \frac{2m_e e^2}{\hbar^2}\left[\frac{\{Z - f^x(k)\}}{k^2}\right] \qquad (4.24)$$

where $f^e(k)$ is the electron scattering factor, m_e is the electron mass, Z is the atomic number, $f^x(k)$ is the X-ray atomic scattering factor. Scattering formalism again remains the same as for as the other two (X-rays and neutrons). The form factor is high compared to X-rays because of the

strong columbic interaction of electrons with both the electrons and nuclei of the atoms. The samples used for electron scattering work, however, have to be very thin because of both pronounced inelastic processes and multiple scattering. A good example of the use of electron diffraction in determining RDF is that of $96B_2O_3 \cdot 4TeO_2$ glasses, which is shown in Figure 4.07. RDF obtained with powdered samples in electron diffraction

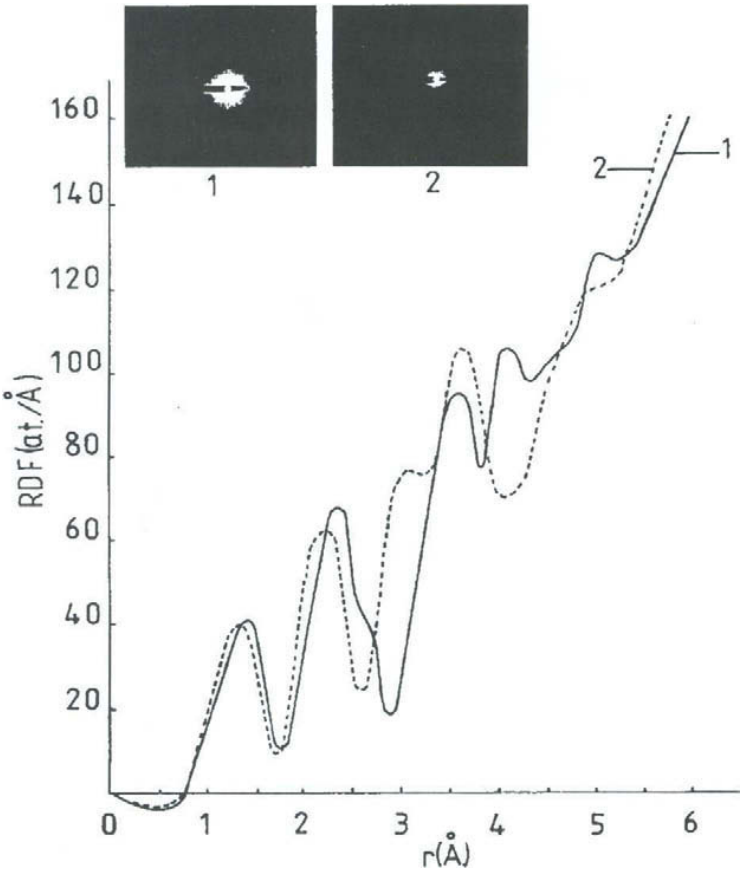

Figure 4.07: RDF curves for powdered samples of (1) B_2O_3 glass and (2) B_2O_3. 4 TeO_2 glass (After Bursukova et al, 1995). 96

studies is also shown in Figure 4.07 for comparison. The differences between the two RDFs is attributed to greater disorder in the case of thin films. The merits of three diffraction techniques are compared in Table 4.1.

All the scattering expressions discussed above are relevant for single component materials. But most glasses are multicomponent materials and consist of several atoms with different scattering factors. In a material consisting of n different atoms, there are $n(n\text{-}1)/2$ pair correlation functions and each of them contribute to the observed scattering intensities.

Table 4.1: Advantages and disadvantages of various scattering techniques (After Elliott, 1984).

Techniques	Advantages	Disadvantages
X-rays (fixed λ, variable θ)	Convenient laboratory sources and equipment. Powdered or thick samples can be used. Atomic form factor can be calculated.	Small k_{max} for many X-ray sources. Significant Compton contribution to scattering at large k. Partial correlation functions difficult to extract for multicomponent systems. Atomic form factor strongly decreasing function of k.
Neutrons (fixed λ, variable θ, double or triple axis)	Scattering length independent of k. Partial correlation functions easier to extract for multicomponent systems. Isotopic substitution possible to determine partial correlation functions.	Reactor source required. Placzek corrections required for double-axis experiments (static approximation). Large volume of material required. b must be determined.
Neutrons (fixed λ, variable θ, time of flight)	(In addition to the above) Large values of k_{max} attainable. Fixed geometry simplifies experiment set-up, e. g. for pressure studies. Simultaneous collection of data for all k-values facilitates time-resolved experiments. Higher count rates (if LINAC used).	Pulsed source required (chopper + steady-state reactor or LINAC source).
Electrons (fixed λ, variable θ)	Uses scanning electron microscope. In situ grown thin films can be examined. High count rates.	Scattering very strong and multiple scattering important for thickness greater than 100 Å. Thin films may not be representative of the bulk structure. Large inelastic scattering background (due to plasmons, etc.)

Generalized XRD intensity function for an n component polymeric system is given by,

$$\frac{I_{eu}}{N} = \sum_{i=1}^{n} x_i f_i^2 + \sum_{i=1}^{n}\sum_{j=1}^{n} x_i x_j f_i f_j \int_0^{\infty} \frac{4\pi r^2 \rho_{ij}(r)}{x_j} \frac{\sin kr}{kr} dr - \left[\sum_{i=1}^{n} x_i f_i\right]^2 \int_0^{\infty} 4\pi r^2 \rho^0 \frac{\sin kr}{kr} dr \quad (4.25)$$

where x_i is the atomic fraction of element i and f_i is the form factor of element i and $\rho_{ij}(r)$ is the average number of j atoms per unit volume at distance r from ith atom. Reduced scattering intensities can be obtained from the above expression.

A single X-ray scattering experiment will not enable determination of all the pair correlation functions or the partial structure functions because a single Fourier transform of the experimentally obtained $F(k)$ functions will not enable individual $\rho_{ij}(r)$ to be determined from such experiment. As a matter of fact using weighted f over the entire range of k is itself strictly incorrect. However in the case of neutron diffraction the k (or Q) independence of $\bar{b}$ is an advantage in deriving the RDFs. Even then assumption has to be made regarding the distribution of the atomic species or the function $\rho_{ij}(r)$. Partial structure factors are given in neutron scattering experiment by suitable isotope substitution because the scattering lengths can be varied without affecting the chemistry and also it is reasonable to assume that isotope substitution does not alter the structure. Since some of the elements allow the change of even the sign of $\bar{b}$ during isotope substitution (see Figure 4.04), it enables determination of individual pair correlation function in neutron scattering. In general $n(n\text{-}1)/2$ pair correlations to be determined increases the complexity and number of experiments to be performed.

In just a binary metallic glass such as $Ni_{81}B_{19}$, it needs 3 isotopic substitutions to evaluate all the three correlation functions. $Ni_{81}B_{19}$ is also a good example of the successful application of neutron diffraction technique and the determination of all the three partial structure factors using isotopic substitution are shown in Figure 4.08.

Particular pair correlation function among a number of pair correlation functions can possibly be determined by isomorphous substitution, that is, by substituting one element by another chemically similar element. The implied assumption is that the structure around the atoms of the given element is not altered. There are also other methods

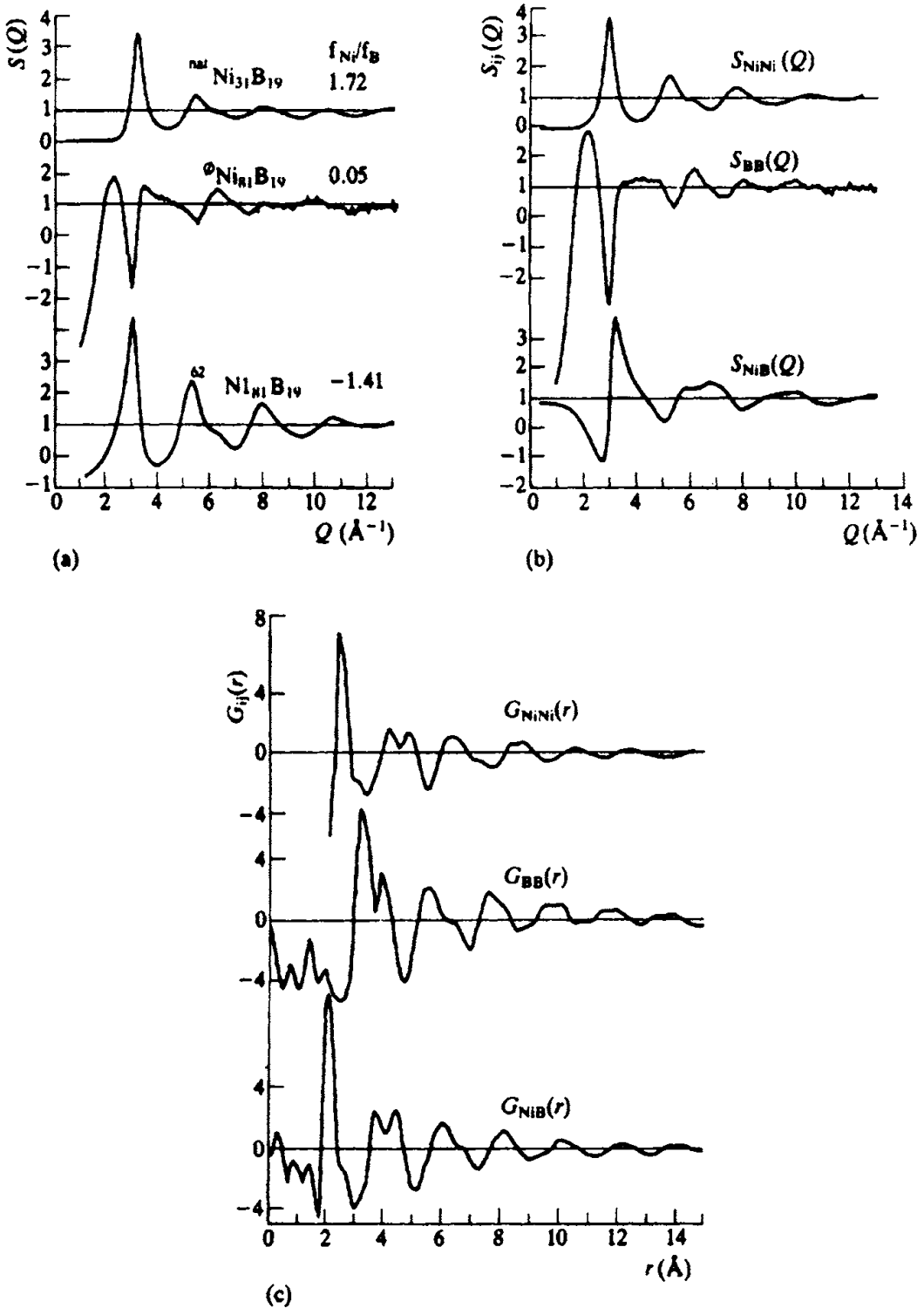

Figure 4.08: Structural studies of $Ni_{81}B_{19}$ using isotopic neutron diffraction; (a) Structure factor for different isotopically substituted alloys. (b) Partial structure factors obtained form those shown in (a). (c) Partial reduced RDFs obtained by Fourier transformation of the $S_{ij}(Q)$ shown in (b) (After Lamparter et al., 1982).

like use of anomalous scattering in X-ray diffraction method, where the scattering factor of a given atom is not only dependent on k but is also dependent on the energy of the X-ray photon. This is because X-ray scattering varies anomalously near the absorption edge. $f(k)$ becomes $f(k,\omega)$ and can be represented as,

$$f(k,\omega) = f^0(k) + f'(k,\omega) + if''(k,\omega) \tag{4.26}$$

The first term f^0(k) is the X-ray atomic scattering factor and the other two terms are the dispersion corrections. Similar anomalous scattering occurs for neutrons also and the neutron scattering factor is formulated in a similar way.

Extended X-ray Absorption Fine Structure

From preceding section, we note that the structural information obtainable from X-ray, neutron and electron scattering techniques is largely limited to obtaining RDF. The RDFs so determined are convolutes of a number of pair correlation functions except in the simplest case of A_mB_n which consists of three pair correlation functions, A-A, B-B and A-B and where three different diffraction experiments can be designed. The task of obtaining individual pair correlations is very difficult. A technique which enables acquiring structural information more directly around a given chemical element is the analysis of "Extended X-ray Absorption Fine Structure" or "EXAFS". It will soon become evident that EXAFS is element specific. It involves ionisation of a core electron of a given atom which propagates outwards from the atom and in the process undergoes diffraction by being scattered from the neighbouring atoms in the structure. The return of the scattered waves affect the absorption coefficient of the given atom, as a result of which the absorption coefficient exhibits undulations. These undulations constitute the EXAFS. Therefore EXAFS technique is the one, which involves diffraction of *in situ* generated low energy electrons. The observed intensity function has built into it a Fourier transform relation to the structure, and therefore, the structure is obtainable through Fourier transform of the observed EXAFS.

Consider X-rays incident on an atom A in a glass such as A_mB_n. The absorption coefficient, μ, for X-rays can be plotted for as a function of photon energy ($\hbar\omega$), an example of which is shown in Figure 4.09. When the energy of the photon corresponds to the binding energy of a core electron like $2p$, $2s$ or $1s$ of the element A, the absorption coefficient

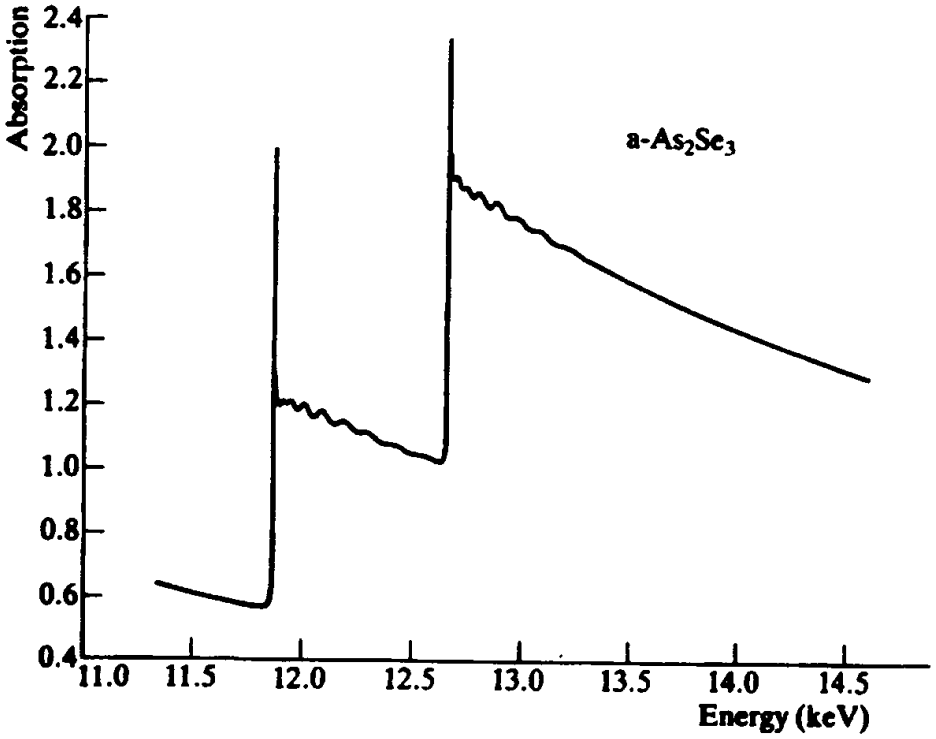

Figure 4.09: Extended X-ray absorption fine structure for a-As_2Se_3 showing the fine structure beyond the As and Se K edges (From Elliott, 1984)

suddenly peaks up. Following every peak absorption there are EXAFS undulations in absorption coefficients. The amplitude of the undulations falls off with increasing energy. The magnitudes of the EXAFS undulations are calculated using the formula,

$$\chi(E)=\frac{\mu(E)-\mu_o}{\mu_0} \quad \text{or} \quad \chi(k)=\frac{\mu(k)-\mu_0}{\mu_0} \tag{4.27}$$

where μ_0 is the background absorption (often one uses $\mu_0 M(k)$ in the denominator where $M(k)$ is known as McMaster correction term).

The origin of the undulations can be understood with reference to Figure 4.10. The X-ray photon liberates a photoelectron from one of the core states (say). This liberated electron propagates as a spherical wave outwards from A, as indicated in Figure 4.10. The propagating wave is now diffracted by the surrounding atoms, which also consists of electrons and nuclei. The phase of the diffracted wave depends on the state of its incidence on the neighbouring atoms. Thus the diffracted wave now returns to the origin in general with a difference in phase and amplitude. It would be instructive to imagine an experiment in which the photoelectron

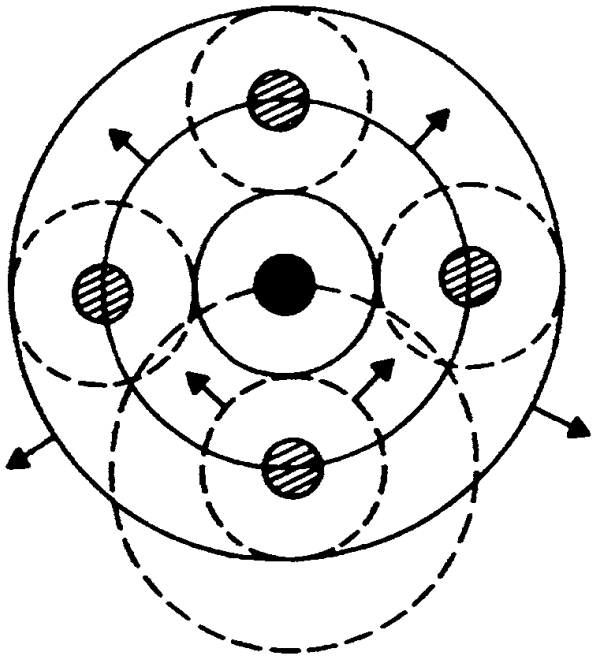

Figure 4.10: Schematic illustration of the EXAFS process.

is ejected with constant energy and the distance of the scatterer is gradually increased. If the wavelength of the photoelectron is λ, then varying the position of the scatterer by a distance λ, the reflected wave will return to the origin with phase differences covering all the values from 0 to 2π. In an actual experiment the distance is not varied, instead, the photoelectron energy or its wavelength itself is varied and the phases of the reflected waves are affected in the same manner.

The superposition of the outgoing and incoming waves alters the wave function of the photoelectron at the site of the given emitter. The final state wave function, $|f\rangle$, becomes $|\varphi_e\rangle + |\varphi_{sc}\rangle$ where φ_e and φ_{sc} are the emitted and scattered wave functions. The photoelectron absorption process involves the final state wave function and the quantum mechanical expression for the X-ray absorption coefficient is given by,

$$\mu = 4N_0\pi^2 e^2 \frac{\omega}{c} \left| \langle f|z|i\rangle \right|^2 \rho(E^f) \tag{4.28}$$

where e is the electronic charge, ω is the X-ray frequency, c is the velocity of light, N_0 is the number density of the absorbing atoms and $\rho(E^f)$ is the density of the final states $|f\rangle$. $\rho(E^f)$ generally varies monotonically because these are free electrons of low energy propagating through the

medium. $|i\rangle$ is the initial core state which is also a smoothly varying function. Therefore the undulations or the oscillatory behaviour of μ in EXAFS can only arise from $|f\rangle$. This, as noted, is a consequence of superposition of propagating and back scattered waves.

Theoretical expression for $\chi(k)$ was derived by Sayers et al. (1971) using single scattering formalism and back scattering of planar waves from shells of atoms surrounding a given emitter and it is given by,

$$\chi(k) = -\sum_j \left(\frac{N_j}{R_j^2}\right)\frac{|f_j(\pi)|}{k}\exp\left(-\frac{2R_j}{\lambda_e}\right)\exp\left(-2\sigma_j k^2\right) .\sin\left(2kR_j + 2\delta(k) + \eta_j(k)\right) \tag{4.29}$$

The sum taken over all back scattering atoms in a shell indexed by j and containing N_j atoms at a distance R_j. It should be noted carefully that the magnitude of the EXAFS is proportional to N_j, which is the number of back scattering atoms and it is inversely proportional to R_j^2, because, the amplitude of the outgoing wave has decreased by $1/R_j$ while going out and once more by the same factor as it returns to the emitter. The back scattering amplitudes $f_j(\pi)$ is in general complex and therefore its magnitude is used. The amplitude of the outgoing wave is also generally attenuated because of the finite mean free path, λ_e, of the electrons (~2000 Å) and the effect is taken care of by the term, $\exp(-2R_j/\lambda_e)$, which has only a very weak influence on the amplitude. σ_j is the root mean square displacement which expresses the static or thermal disorder about the equilibrium bond length and is the Debye Waller factor. The sinusoidal function expresses the influence of the phase shift of the electron on μ and consists of three terms for a given value of k or the energy of the photon. First term is $2kR_j$ indicating the influence of emitter scatterrer distance, R_j. The second and third terms ($\delta(k)$ and $\eta_j(k)$) arise because the photoelectron is emitted and back scattered respectively under the influence of emitter-scatterer potentials. The wave number of the photoelectron is given by,

$$k = \frac{2\pi}{\lambda} = \left[\frac{2m_e(E - E_0)}{\hbar^2}\right]^{1/2} \tag{4.30}$$

where E_0 is the threshold energy. Thus the above expression consists of N_j, R_j and σ_j which are structural parameters to be determined from EXAFS

and f_i, ϕ_j (the phase term $2kR_j+2\delta(k)+\eta_j(k)$) and λ_e which are the scattering parameters. In actual EXAFS experiments $\chi(k)$ is determined using equation (4.27) up to as high a value of energy as possible, but starting with at least 30-40 eV above the edge (k values of ~ 4 and above). This is because for energies lower than 30-40 eV multiple scattering becomes dominant and also the assumption of a planar wave in the derivation of equation (4.29) is not strictly valid. In fact it is safe to consider EXAFS undulations as only those, which occur above 80 eV from the edge. The amplitude parameters have been theoretically calculated and listed as functions of k for various atoms. η and δ are not generally available as they are material dependent. The most widely used procedure involves use of Fourier transformation technique, where the Fourier transform yields $\phi(r)$ which is a radial function. It is in principle a pair distribution function and is given by

$$\phi(r)=\left(\frac{1}{2\pi}\right)^{1/2}\int_{k_{\min}}^{k_{\max}}\chi(k)M(k)k^n\exp(2ikr)dk \tag{4.31}$$

$M(k)$ is a window function and k^n is k weighing used with $\chi(k)$ which enhances the weightage of amplitude in $\chi(k)$. This helps in obtaining better Fourier transform. Since $\exp(2ikr)$ ignores η and δ, the peaks obtained in $\phi(r)$ do not represent true distances and are shifted. In order to overcome this problem $\chi(k)$ is obtained for a known crystalline solid for the same emitter-scatterer atom pairs so that the phase shifts (and if necessary even amplitudes) are fixed on the basis of the analysis of the crystal data. These phase shifts are then assumed to be transferable so that $\chi(k)$ of the given glass is fitted with such phase parameters. The phase and amplitude parameters, however, have been determined from first principles for several glasses (Gurmann and Pettifier, 1979).

In general, EXAFS can be carefully analysed to obtain distances of first and second neighbours to within ± 0.01Å. But N_j (j = 1) can be accurate up to only ± 20 %. In the analysis of glass structure, EXAFS has a very important role because with the availability of synchroton radiation, core electrons of most of the elements can be excited from $1s$, $2s$ or $2p$ (two) states. In fact these edges are known as K, L_1, L_2 and L_3 edges respectively. It is possible to study even M edge spectra for suitably chosen elements. The K, L_1 and L_2 edge spectra of Nd in fluoroberyllate glasses studied by EXAFS is shown in Figure 4.11. The general procedure

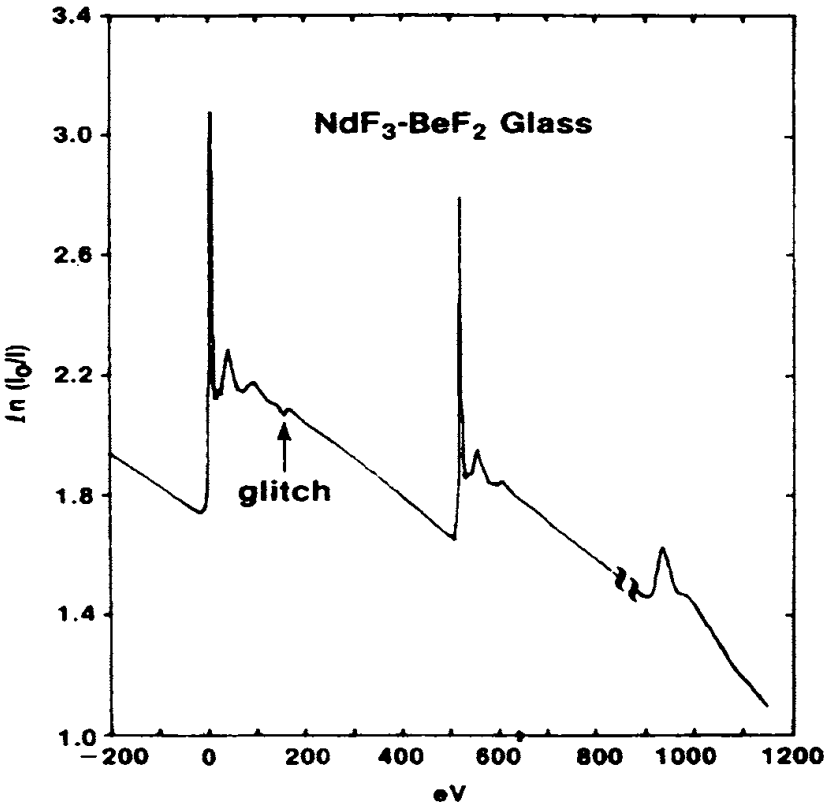

Figure 4.11: Room-temperature experimental XANES and EXAFS scans of BeF_2 glass containing 4 mol % Nd at the Nd L_3, L_2 and L_1 edges (After Rao et al., 1983).

adopted in the analysis of EXAFS is represented in Figure 4.12. The "raw" $\chi(k)$ obtained from the spectra like in Figure 4.11 is converted into a k-weighted EXAFS, $k^n \cdot \chi(k)$. In Figure 4.12(a), n = 1 and $k \cdot \chi(k)$ has been plotted as a function of k. The Fourier Transform of this is shown in Figure 4.12(b), which is the RDF. It consists of various peaks and each peak in principle represents a shell and the distances to various neighbours can be thus determined. But the distances are generally smaller because of the k weighting of the $\chi(k)$ before Fourier transformation. One of the widely used procedures is to recover $k^n \cdot \chi(k)$ for the individual peaks – generally the first peak - by inverse FT of the "windowed" peak (between the lowest values of RDF on either side of the peak). Having recovered $k^n \cdot \chi(k)$ it is now fitted for theoretical EXAFS using scattering parameters as inputs and adjusting the structural parameters (a least squares fitting procedure is adopted). Phase parameters in fitting the data for Figure 4.12(c) were determined from the data on crystalline NdF_3. The quality of the fit determines the accuracy of the structural parameters. In the present case, N_j of Nd was found to be ~ 7 and distances vary from 2.33-3.04 Å.

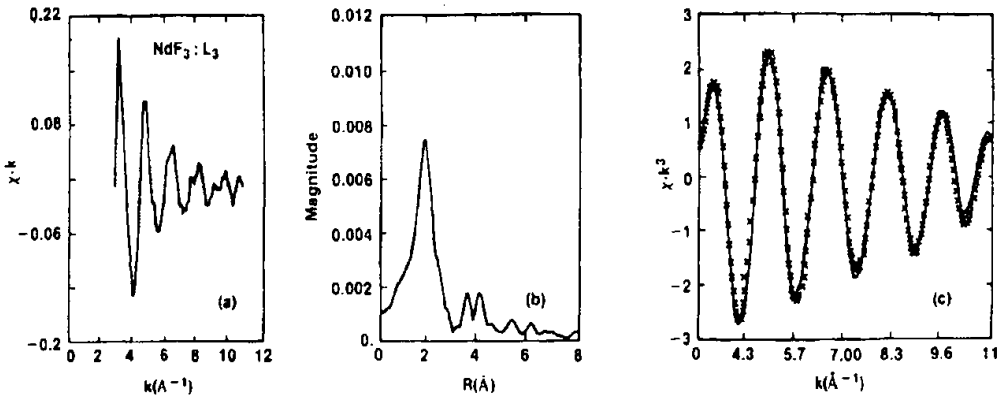

Figure 4.12: (a) Normalized Nd L_3 EXAFS for crystalline NdF_3; (b) Fourier transform of (a) and (c) inverse transform (line) and simulated EXAFS (points) in the region 0.2 to 3.2 Å (After Rao et al, 1983).

One of the serious limitations of EXAFS technique is with regard to phase parameters. These are quite generally obtained from analysis of EXAFS of crystalline compounds of known structure. In order that such phase information be transferable, the structure around the given atom should be very similar. This admittedly is a weakness because the structure of the glass is clearly unknown. Further use of these phase parameters in fitting the experimental EXAFS of a glass imposes a genetic influence on the structure in the sense that it tries to fit the EXAFS of unknown with as many subshells of atoms (as many sets of phase parameters) as there are in the model crystalline compound.

X-ray Absorption Near Edge Structure

XANES is the acronym for X-ray absorption near edge structure. In principle it should include absorption features, which are described as both pre-edge and post-edge. Glasses consisting of transition metal ions often exhibit sharp pre-edge absorption just before the major X-ray absorption peak. On the high energy side of the major peak is the EXAFS. The peaks are attributed to excitations to bound states. These bound states can be low lying bonding and antibonding states in many atoms or the crystal field split vacant levels of the transition metals or they can be unoccupied Rydberg states of the ion below the ionisation potential. The allowed core electron excitation ($s \rightarrow p$ or $p \rightarrow d$ etc.) gives rise to sharp features. A well studied example of excitation to crystal field split levels is that of Ti and is given in Figure 4.13. There is a pre-edge peak attributed to $1s \rightarrow 3d$ transition in the K edge spectra. This peak is sensitive to local

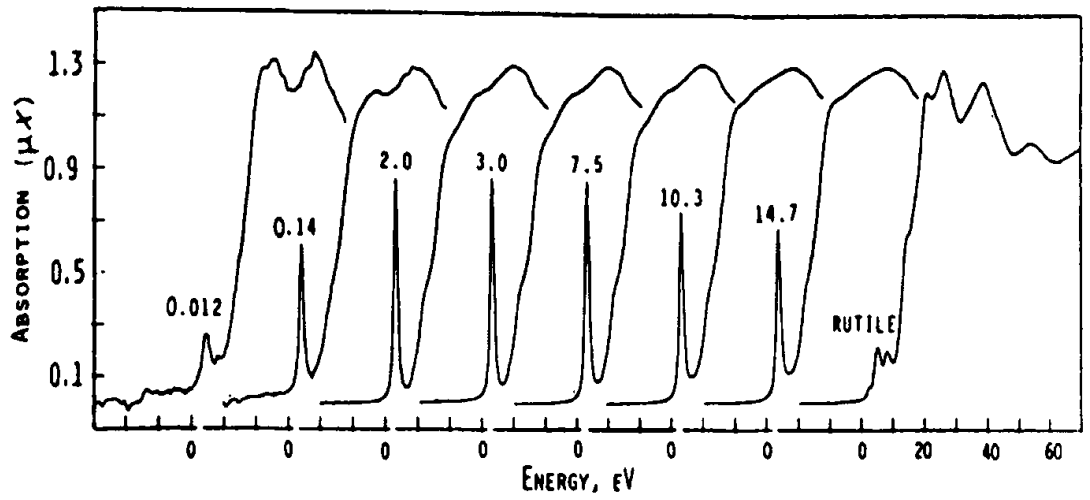

Figure 4.13: The near-edge K absorption spectra of a series of TiO_2-SiO_2 glasses plus a standard material, rutile, TiO_2. The concentration of TiO_2 is labelled in wt % (After Lewis, 1989).

symmetry being absent in rutile but present in anatase. In several cases these so-called pre-edge phenomena merge with the main threshold absorption and become indistinguishable, primarily because of poor resolution, inadequate to observe such bound state to bound state excitations. If the absorption is an allowed transition to vacant *p* or *d* state, the absorption can be sufficiently intense. Immediately next to absorption edge also a few absorption coefficient undulations are observed. The peaks close to the absorption edge are likely to arise from excitation to allowed bound states and an analysis of the structure of near edge can yield valuable information on the symmetry of the ligand ions. This is fairly clearly observed when the excitation occurs from 2*p* core level to vacant *nd* levels; the splitting of *nd* levels determines the number of peaks in the XANES, while the splitting itself is a consequence of the crystal field symmetry around the atom. While T_d or O_h symmetries lead to two split levels, lower symmetries can give rise to more. Let us suppose that the analysis of EXAFS associated with the same edge reveals the presence of 4 or 6 nearest neighbours. It is suggestive of a crystal field geometry of T_d or O_h respectively around the given ion if the XANES has just two sub peaks (can be often seen in derivative XANES spectra). Thus a combination of EXAFS and XANES in such cases can be a very powerful tool for the study of SRO. However, XANES is viewed as low energy portion of EXAFS itself for which the single scattering formalism is inadequate and is therefore left out of the analysis. Care is hence necessary in the analysis of near edge data.

Nuclear Magnetic Resonance

Structural investigations in glassy state, particularly in the regime of SRO, has been helped tremendously by the technique of nuclear magnetic resonance (NMR). Several important elements frequently found in glasses fortunately possess nuclear magnetic moment, such as for example B, Al, Si, O, Li, F, Pb, Te, Sn etc. Proton and carbon which are constituents of all organic glasses also possess nonzero spin. The nuclear spin values and natural abundances of these elements are listed along with their Larmour frequencies in Table 4.2.

The basis of application of NMR technique (Fyfe, 1983) is that the degenerate nuclear spin levels of atoms are split when an external magnetic field is applied – due to Zeeman interaction. If I is the nuclear spin which may be integral or half integral, it splits into equally spaced $(2I+1)$ states in a magnetic field. If the strength of the magnetic field is H, then the separation of the energy levels is given by ΔE, and

$$\Delta E = \gamma.\hbar H \tag{4.32}$$

where γ is the gyromagnetic ratio of the nuclei and $\hbar\,(= h/2\pi)$ is the Planck constant. The spins are distributed into various Zeeman split states following a Boltzmann distribution law. If the system is now irradiated with electromagnetic radiation of frequency ν_0 such that $h\nu_0=\Delta E$, then the spins in the lower energy states absorb the energy and get excited to higher energy. Under the ideal condition, i.e. in the absence of any other interaction, a sharp absorption peak is expected to be present in its NMR absorption spectrum. It is illustrated in Figure 4.14 schematically for the case of $I = 3/2$. In the actual spectrum, the absorption peaks are not sharp delta functions (Figure 4.14 (b)) but are broadened peaks as illustrated in Figure 4.14 (c). This is due to several interactions of the magnetic moments of the nuclei, which affect the splitting. The most important of them is the dipolar interactions. The magnetic moment, $\vec{\mu}$ is a vector given by,

$$\vec{\mu} = \gamma.\hbar\vec{I} \tag{4.33}$$

Two dipoles $\vec{\mu}_1$ and $\vec{\mu}_2$ are situated at a distance r_{12} interact with an energy proportional to $(\vec{\mu}_1.\vec{\mu}_2)/r_{12}^6$. The dipolar interactions have the effect of broadening the resonance frequencies. The magnitude of this

Table 4.2: Characteristic nuclear properties of various elements. (After Zarzycki, 1982)

Nuclei	Natural abundance %	Larmour frequency MHz (at 10^4 Gauss)	Magnetic moment (in nuclear magnetons)	Spin (in ħ units)	Electric quadrupole moment (10^{-24} cm^2)
^{1}H	99.9844	42.577	2.7927	½	-
^{7}Li	92.57	16.547	3.2560	3/2	-4.2×10^{-2}
^{9}Be	100	5.983	-1.7740	3/2	2.0×10^{-2}
^{11}B	81.17	13.660	2.6880	3/2	3.55×10^{-2}
^{19}F	100	40.055	2.6273	1/2	-
^{23}Na	100	11.262	2.2161	3/2	0.1
^{27}Al	100	11.094	3.6385	5/2	0.149
^{29}Si	4.70	8.460	-0.55477	1/2	-
^{31}P	100	17.235	1.1305	1/2	-
^{45}Sc	100	10.343	4.7491	1/2	-
^{51}V	~ 100	11.193	5.1392	7/2	0.3
^{73}Ge	7.61	1.485	-0.8768	9/2	-0.2
^{75}As	100	7.292	1.4349	3/2	0.3
^{111}Cd	12.86	9.028	-0.5922	1/2	-
^{113}Cd	12.34	9.444	-0.6195	1/2	-
^{125}Te	7.03	13.45	-0.8824	1/2	-
^{133}Cs	100	5.585	2.5642	7/2	< 0.3
^{205}Tl	70.48	24.57	1.614	1/2	-
^{207}Pb	21.11	8.899	0.5837	1/2	-

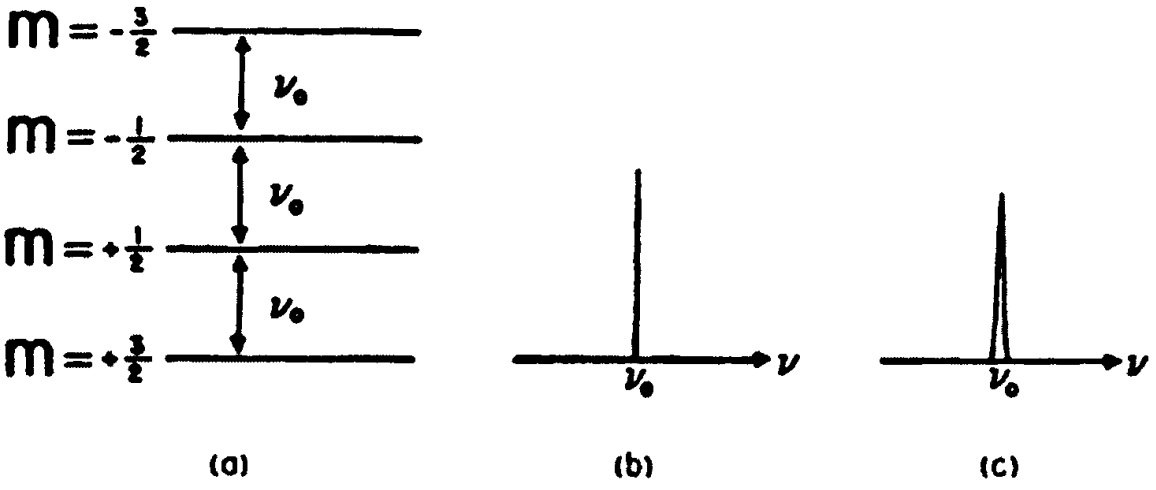

Figure 4.14: (a) Energy levels for a spin 3/2 nucleus in the presence of a magnetic field. (b) The resultant NMR absorption spectrum in a single peak at the frequency ν_0. (c) Dipolar interactions broaden the resonance symmetrically so that it is not the delta-function response depicted in (b).

broadening contribution to the full width at half maximum (FWHM) of a resonance peak can be calculated using van Vleck's (1948) method. This dipole-dipole contribution, δ, is given by,

$$\delta = 2.36\sqrt{M_2^I} \tag{4.34}$$

where M_2^I is the second moment of the nuclear spin. If there are spins with two different values, say I and I', then M_2^I is a sum of two terms:

$$M_2^I = \Delta_{I,I} + \Delta_{I,I'} \tag{4.35}$$

where

$$\Delta_{I,I} = \frac{3}{5}\gamma_I^4 \hbar^2 I(I+1)\sum\left(\frac{1}{r^6}\right) \tag{4.36}$$

and

$$\Delta_{I,I'} = \frac{4}{5}\gamma_I^2 \gamma_{I'}^2 \hbar^2 I'(I'+1)\sum\left(\frac{1}{r^6}\right) \tag{4.37}$$

Of greater interest to the chemistry of glasses is the chemical shift interaction term. This arises from the fact that the extra nuclear electrons in the atom also respond to the applied magnetic field by virtue of which they shield the nucleus from the external magnetic field. As a consequence, a small shift occurs in the resonance frequency and this is known as the chemical shift. It is measured in parts per million (ppm). The chemical shift interaction energy, E_{CS} can be written as,

$$E_{CS} = \gamma \hbar \vec{I} \tilde{\sigma} \vec{H} \tag{4.38}$$

Where $\tilde{\sigma}$ is the chemical shift tensor. The observed resonance frequency ν is given by,

$$\nu = \nu_0(1-\sigma_{zz}) \tag{4.39}$$

where σ_{zz} is the component of the chemical shift tensor in the direction of

the applied field. If the diagonal elements of the chemical shift tensor along the principal axes are represented for convenience as σ_1, σ_2 and σ_3, ν for arbitrary orientation is given by,

$$\nu = \nu_0[1 - \sigma_{iso} - \sigma_{axial}(3\cos^2\theta - 1) - \sigma_{aniso}(\sin^2\theta \cos 2\phi)] \tag{4.40}$$

where σ_{iso} and σ_{aniso} are the isotropic and anisotropic chemical shift values. In terms of σ_1, σ_2 and σ_3,

$$\begin{aligned} \sigma_{iso} &= \frac{1}{3}(\sigma_1 + \sigma_2 + \sigma_3) \\ \sigma_{axial} &= \frac{1}{6}(2\sigma_3 - \sigma_1 - \sigma_2) \\ \sigma_{aniso} &= \frac{1}{2}(\sigma_2 - \sigma_1) \end{aligned} \tag{4.41}$$

θ and ϕ are the polar angles of the field H with respect to the principal axis of the chemical shift tensor. In a glass or a powdered sample, all orientations are possible and therefore the spectrum is an envelope of the responses for all values of θ and ϕ. The theoretical powder patterns appear as shown in Figure 4.15. The sharp shoulders and the divergences are smoothened out in the real spectrum due to dipolar interaction.

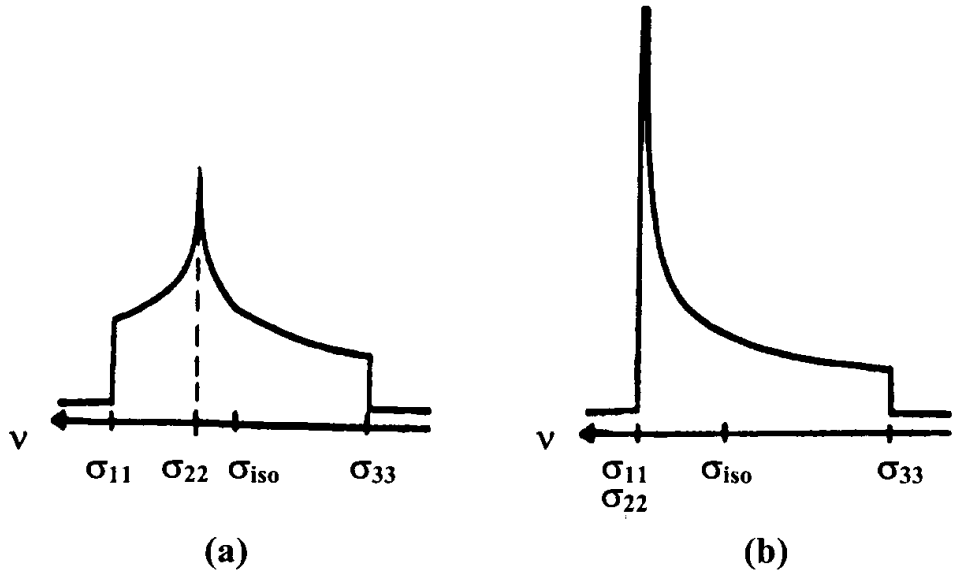

Figure 4.15: Chemical shift powder patterns for (a) asymmetric and (b) axially symmetric anisotropies (After Emerson and Bray, 1993).

Another important interaction which contributes to broadening of resonance peaks is the quadurpolar interaction. When the nuclear spin, $I \geq 1$, the nuclei possess electric quadurpole moment, eQ. The quadurpole moment Q is a measure of the distortion of spherical symmetry of the nuclear charge distribution. Quadurpole moment interacts with the electric field gradient, EFG, present at the nucleus. These are the fields caused by the electrons in the atom. Spherical distribution of electrons in closed shells do not produce any EFG at the nucleus but the bonding electrons do. Therefore the quadurpolar interaction can be used to obtain information on chemical bonding. Quadurpolar interaction shifts the Zeeman levels. The first order correction due to quadurpolar interaction to the Zeeman splitting between levels m and (m-1) is given by,

$$\nu_{m\to m-1} = \nu_0 - \nu_Q\left(\frac{m-(1/2)}{2}\right)\left[(3\cos^2\theta - 1) - \eta\sin^2\theta\cos 2\phi\right] \tag{4.42}$$

where

$$\nu_Q = \frac{3Q_{CC}}{2I(2I-1)} \tag{4.43}$$

and Q_{cc} is the quadurpolar coupling constant, given by

$$Q_{cc} = \frac{eQV_{zz}}{H} \tag{4.44}$$

Where V_{zz} is the principal axes component of the EFG tensor. The asymmetry parameter, η, is a measure of the departure of EFG from cylindrical symmetry.

$$\eta = \frac{(V_{xx} - V_{yy})}{V_{zz}} \tag{4.45}$$

such that $0 \leq \eta \leq 1$. θ and ϕ are, as noted earlier, polar angles of the magnetic field with respect to the principal axes of the EFG tensor. Therefore the spin bearing nuclei have both field dependent and field independent (zero field) terms, which determine the energy states and their splitting.

The nuclear Hamiltonian relevant for NMR studies is therefore given by

$$H_{NMR} = -\gamma \hbar \vec{I} \vec{H} + \gamma \hbar \vec{I} \tilde{\sigma} \vec{H} + \vec{I} \tilde{D} \vec{I} + \vec{I} \tilde{Q} \vec{I} \qquad (4.46)$$

In equation 4.46 the first term represents the Zeeman splitting, second the chemical shift, third the dipolar and fourth the quadurpolar terms. NMR spectrum of nuclei in the liquid state are very sharp while they are very broad in the solid state. This is largely due to the third term which is due to dipole-dipole interaction. In liquids there is a natural freedom for atoms and molecules to take any orientation so that dipolar interactions average out, but this is not the case in solids. Thus all the anisotropic interactions in liquids essentially become zero and the observed line widths in NMR are of the order of 1 Hz which arises from the magnetic field inhomogeneity. The large widths of the order of several kHz observed in solids arise from these anisotropic interactions. The first attempt to overcome this problem was made by Andrew et al. and independently by Lowe in 1959 by using a specimen rotation technique, known as magic angle spinning (MAS) NMR. When carefully examined, the interaction terms in equation (4.44) which are sources of anisotropy and broadening reveal that they consist of a term, which is $(3\cos^2\theta_{ij} - 1)$, where θ_{ij} is the angle between the magnetic field direction and the internuclear vector. Therefore, when this angle, $\theta = 54°44'$, all the anisotropic terms become zero and NMR signal should become narrow. What is required therefore is to spin the sample at that angle of 54°44′ with respect to field direction. In particular the broadening caused by dipolar interaction is completely removed by such spinning. It has been shown that broadening due to chemical shift anisotropy is also removed so that the resulting narrow lines in the NMR spectrum can be used to identify different chemical environments of the nuclei. In order to achieve very narrow lines the rate of rotation must exceed the line widths, otherwise the transfer magnetization decays faster than the time it takes to complete one revolution and this results in the retention of broadening.

There are other methods of analysis of NMR of glassy solids such as the broad line or continuous wave NMR particularly valuable for quadurpolar nuclei like ^{11}B. In Figure 4.16, broad line NMR spectrum of ^{11}B in B_2O_3 glass is presented along with the MAS NMR to illustrate the effect of spinning on the widths of resonance peaks. Comparison is also provided with the MAS NMR of crystalline B_2O_3. Several examples of the

use of MAS NMR in structural investigations are cited in this book in subsequent chapters.

Pulsed NMR spectroscopy (Fukishima and Roeder, 1981; Farrar and Becker, 1971) is another technique very useful in glass science. A short and intense pulse consisting of the entire range of frequencies of interest is used to irradiate the sample. The total magnetisation of the sample gets rotated from its equilibrium position along the z-axis by an angle θ_p, which is given by,

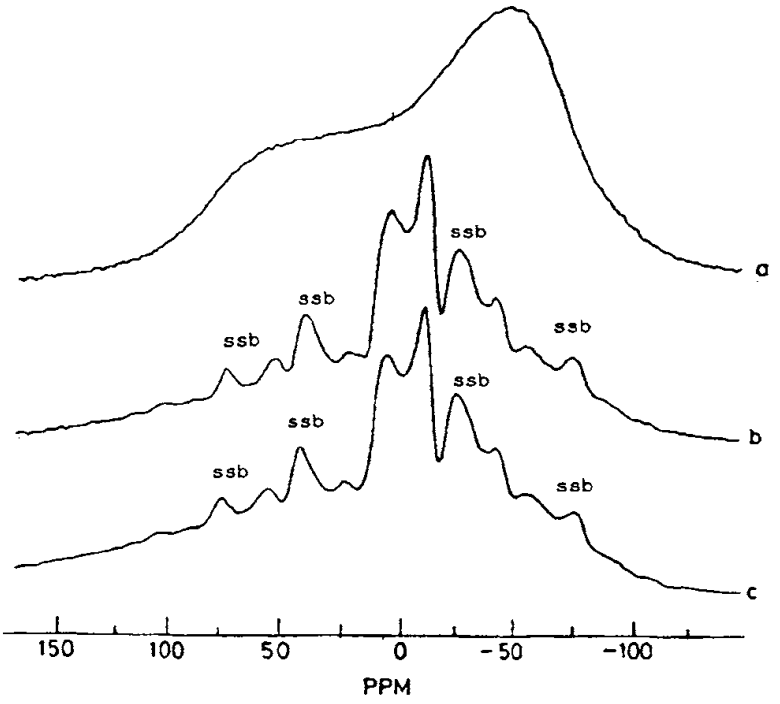

Figure 4.16: ^{11}B NMR spectra of B_2O_3. (a) Powder pattern of glassy B_2O_3; (b) MAS spectra (~ 3 kHz) of glassy B_2O_3; (c) MAS spectra (~ 3 kHz) of crystalline B_2O_3. (ssb, spinning side bands). (After Prabakar et al, 1990)

$$\theta_P = \gamma H_1 t_P \tag{4.47}$$

where the angular frequency is expressed as γH_1 and duration of the pulse by t_p as shown in Figure 4.17. With reference to the figure, the components of the magnetisation vector ($\boldsymbol{M}$) lying in the x-y plane give rise to an induction in a receiver coil. This is designated as the free induction. The pulse induces the alignment of the individual spins, but the interaction between individual spins, spin-spin interaction, causes dephasing, which therefore decreases the magnitude of $\boldsymbol{M}$. The spin-spin interaction is characterized by a time constant T_2 while corresponding spin-lattice time constant is designated as T_1. Spin-lattice relaxation occurs

through a coupling to the phonon spectrum of the material. The effect of the spin-lattice relaxation is to bring down the magnetisation to its equilibrium value and therefore to diminish the free induction. The free induction picked up by the receiver coil decays with time and is appropriately called a free induction decay (FID). With repeated pulses, the corresponding FID signals are accumulated and averaged. It is Fourier transformed and the real part of the FID (which is a complex quantity) gives the NMR absorption spectrum. The decay of the FID is generally

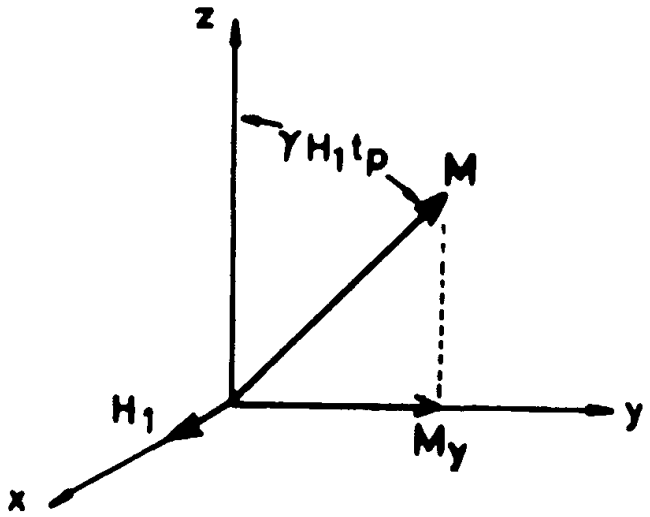

Figure 4.17: A pulse of length, t_p rotates the magnetization vector from its equilibrium position by an angle, $\theta_p = \gamma H_1 t_p$.

exponential and is characterized by the time constant, T_2^* or the apparent T_2, and T_2^* is related to the FWHM as

$$FWHM = \frac{2}{T_2^*} \tag{4.48}$$

T_2^* actually is the total effect of both spin-spin and spin-lattice time constants and is given by,

$$\frac{1}{T_2^*} \approx \frac{1}{2T_1} + \frac{1}{T_2} + \text{a small term} \tag{4.49}$$

The small term is due to the broadening caused by the magnetic field inhomogeneity. In solids, spin-lattice relaxation time, T_1 is much longer

and therefore the free induction decay (FID) gives directly, T_2 as $T_2 \approx T_2^*$. Thus this powerful technique of pulsed NMR gives the important dynamical quantity T_2, which is of particular significance in studying ion transport. It is necessary in such experiments that the pulse rate is adjusted so as to avoid insufficient decay. The inverse of pulse frequency must be significantly higher than T_1. The problem of long T_1 can be circumvented particularly when structural information is required, by putting small paramagnetic species in the sample so that enough FIDs are collected from which the FT yields the necessary spectrum.

A further advance in the use of pulse technique is the spin echo method (Hahn, 1950; Waugh et al., 1968; Mehring, 1978; Emerson and Bray, 1993). Briefly in this technique, a 90^0 pulse is applied at $t = t_0$. 90^0 pulse is that for which $\theta_p = \pi/2$. This causes an induction, which then dephases and begins to decay. After a time τ, a 180^0 pulse is imposed, which now rotates the spins by 180^0. As a consequence, the same mechanism which was responsible for dephasing of spins in the xy plane, now acts to rephase the spins. After a time interval of 2τ, a spin echo is formed. The spin echo therefore represents cumulative action of two FIDs taking place from opposite directions. The FT of the second half of the spin echo gives the absorption spectrum.

MAS NMR often consists of a number of resonances of similar structure on either side of the main signal. While the main resonance peaks remain unaffected by the spinning speed in terms of their chemical shifts, these similar looking features on either side of the main resonance shift for different spinning speeds. These are known as 'spinning side bands' or SSBs. Large SSB intensities are an indication of particularly high degree of chemical shift anisotropy.

Another important observation in the NMR spectra of glasses (also of several crystalline solids) is the so-called motional narrowing effect. The resonance peaks become narrow (FWHM decreases) in the wide line NMR (NMR spectrum obtained without spinning) when the temperature is increased. A typical example is ^{7}Li NMR in Li^+ ion conducting glasses. ^{7}Li NMR is particularly helpful in determining activation energies for lithium ion motion in glasses. Several theories have been adopted (from the study of similar effects in liquids) or developed to explain the observed motional narrowing effect. A phenomenological equation derived by Hendrickson and Bray (1973) using a two-state model for the diffusing ion has been the most popular. When inhomogeneous broadening is negligible, the narrowing effect can be expressed through the following equation:

$$\ln\left(\frac{1}{\Delta\omega} - \frac{1}{\Delta\omega_0}\right) = -\frac{E_a}{kT} - \ln\left(\frac{1}{B} - \frac{1}{\Delta\omega_0}\right) \tag{4.50}$$

where $\Delta\omega$ is the NMR linewidth at temperature T and $\Delta\omega_0$ is the rigid lattice linewidth, E_a is the activation energy for motion of the ion under consideration and B is a constant. Dominant use of NMR in glasses is in the study of speciation in many complex glass systems. We will discuss in later chapters a number of applications of NMR - particularly MAS NMR - in deducing SRO in glasses.

Vibrational spectroscopy

Infrared (IR) and Raman spectroscopic techniques are widely used in the structural investigation of glasses (Bendow, 1993). These techniques very often provide complementary information. Since there are excellent books (Wong and Angell, 1976; Long, 1977; Fadini and Schneppel, 1989; Mitra, 1969; Balkanski, 1971; Rao, 1963; Sathyanarayana, 1996) and reviews (Lerner and Adar, 1989; Loudon, 1964) on the subject, only a brief introduction to this subject is presented in this section. Both IR and Raman use electromagnetic radiation to probe fundamental excitations such as phonos, plasmons etc. In IR spectroscopy, a direct coupling of the electromagnetic radiation to the dipole moment associated with the vibrational excitation is involved. In the case of Raman scattering use is made of a single frequency of usually visible light, whose inelastically scattered components consist of the information on the phonons of the system. In the technique of IR spectroscopy, continuously increasing wavelengths are made either to pass through the material (transmission mode) or reflected from the surface of the material (reflection mode). Peaks are seen both in absorption and reflection corresponding to the frequencies of vibration in the material. In the Raman scattering, the incident frequencies are shifted both in positive and negative direction by magnitudes corresponding to vibrational frequencies. The negatively shifted frequencies are the Stokes lines and the positively shifted frequencies are the anti-Stokes lines. It is schematically represented in Figure 4.18. Stokes lines correspond to the creation and anti-Stokes to the annihilation of phonons. Theoretical considerations reveal that anti-Stokes lines generally have much lower intensity and the study of Raman (vibrational) spectra is thus the study of the Stokes lines. The origin of Raman spectra can be understood on the basis of first order scattering theory. It precludes non-linear effects, which manifest at higher

intensity of incident radiation. The process involves scattering from phonons of wide energy range originating from various vibrational modes in a given system. They can be very low frequency acoustic modes also. In the experiments the main irradiating light beam itself emerges slightly broadened due to elastic scattering (no energy change), which is the

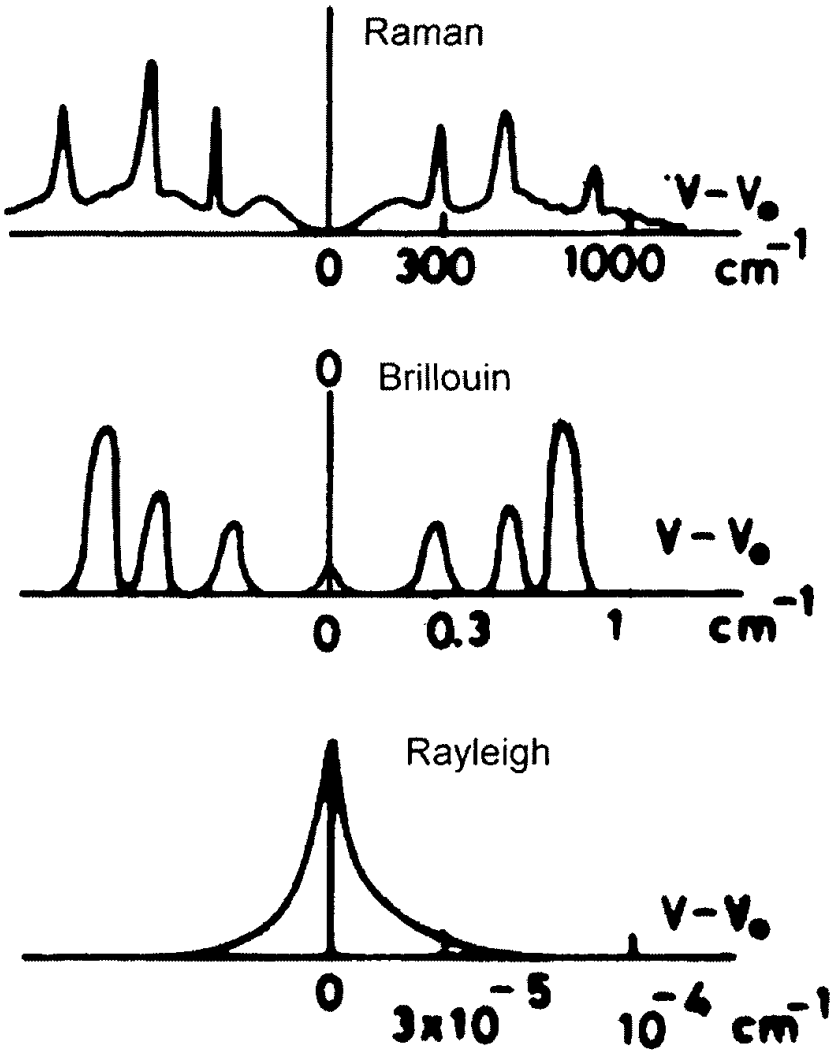

Figure 4.18: Schematic of Raman, Brillouin and Rayleigh scattering spectra in solids, indicating the characteristic frequency ranges for each type of scattering. (After Cummins, 1971)

Rayleigh scattering. The inelastic scattering due to low energy acoustic phonons appear close to the Rayleigh peak and constitute Brillouin spectra. The vibrational modes whose energies are higher are generally

due to either optical phonons or high frequency acoustic phonons and constitute what is generally known as Raman scattering. The widely used configuration for recording Raman spectra is the 90° geometry where the elastically scattered component is absent. Raman and IR spectra provide complementary information about the structure. This is because although they probe the same vibrational frequencies of a material, the selection rules for the Raman and IR spectroscopies are different and therefore the structural details are more completely probed by the use of both the techniques.

It would be instructive to consider the origin of phonons in amorphous solids because the observed characteristic vibrational peaks are sometimes quite sharp in both IR and Raman spectra of many glasses. They are associated with particular chemical or structural species. The question is how is the sharpness of peaks justified. In the simplest case, an isolated molecule can be considered as atoms connected to each other with characteristic force constants. If it is a diatomic molecule with a single spring of force constant, f, with the two atoms vibrating against each other, it is easy to show by setting up the equation of motion that this is governed by the relation

$$\omega_0^2 = \frac{f}{\mu} \tag{4.51}$$

$1/\mu = (1/m_1) + (1/m_2)$, where m_1 and m_2 are the masses of the atoms in the molecule. For larger molecules consisting of several springs and therefore several spring constants, there will be several ways in which the atoms are displaced and therefore several vibrations. Each such set of displacements is designated a vibrational mode and for a molecule containing N atoms, there are $(3N\text{-}6)$ such modes which are independent of each other (meaning, no one mode is described by any combination of other modes). In linear molecules this number is reduced by 1 because of the existence of an axis of rotation, which acts as a constraint. These are also known as normal modes of vibration. The vibrational spectrum of a molecule, in principle, should consist of a set of distinct narrow peaks. Of course, not all the peaks appear both in IR and Raman. Some peaks appear exclusively in either of the spectra. This is because of the selection rules. For a vibrational mode to be IR active it requires that electromagnetic radiation couples directly to the vibrational mode through the coupling of electrical vector of the IR radiation to the dipole moment associated with the vibrational mode. In the simplest diatomic molecule we considered

above, if it is a homopolar diatomic molecule, the only mode of vibration has no dipole moment change and therefore the mode is not IR active. The matrix element for IR absorption will be non-zero only when there is a net dipole moment change. *

IR spectroscopy

The understanding of IR spectra of glasses is helped by first considering the IR spectra of crystalline solids. A crystal corresponds to a 3-*d* periodic array of atoms, ions or molecules connected by springs except that all the spring connectivities repeat themselves from unit cell to unit cell. If it is a molecular crystal such as orthoterphenyl or salol, the intramolecular spring constants (and hence the corresponding interactions) are much higher than the intermolecular spring constants. Therefore the vibrational frequencies within the molecules are much stronger than those between the molecules as they are characterised by van der Waals interactions. In the case of an ionic or covalently bonded crystal, if there are N atoms in the unit cell, there are $(3N\text{-}3)$ vibrational modes, and in the crystal it can be shown that they become $(3N\text{-}3)$ branches in which each branch spans a number of frequencies as a function of wave vector k. The wave vector which characterizes the Brillouin zones restrict the number of vibrational modes in the crystal. A unit cell consisting of two atoms

---

* The general approach to understanding the IR absorption is the same as described under dielectric absorption. The complex dielectric constant $\varepsilon^*(\omega)$ is $\varepsilon^*(\omega) = \varepsilon' + i\varepsilon'' = n^2 - \kappa^2 + 2in\kappa$, where n is the refractive index and κ is the extinction coefficient. The infrared response is characterised through reflectivity R and absorption coefficient, α, given by the relations

$$R = \frac{(n-1)^2 + \kappa^2}{(n+1)^2 + \kappa^2} \qquad \text{and} \qquad \alpha = \frac{4\pi\kappa}{\lambda}$$

The frequency dependent dielectric constant for a damped anharmonic oscillator of characteristic frequency ω_0 and damping constant γ is given by

$$\varepsilon(\omega) = \varepsilon(\infty) + \frac{\varepsilon(0) - \varepsilon(\infty)}{\left(1 - \frac{\omega}{\omega_0}\right)^2 + i\left(\frac{\gamma}{\omega_0}\right)\left(\frac{\omega}{\omega_0}\right)}$$

In the dielectric spectra therefore the IR active mode gives rise to an absorption peak near $\omega=\omega_0$ whose width is proportional to γ. This is the transverse optical (TO) mode. The longitudinal optical (LO) mode appears as a peak in a plot of $1/\varepsilon(\omega)$ vs ω.

therefore leads to the formation of 3 branches; 2 acoustic and one optical. The acoustic branch is that whose frequency becomes zero at $k = 0$ while the optical branch is that whose frequency has a finite value at $k = 0$. In the IR spectroscopy, the wave number of light used being very small the radiation couples to the optical phonons only near $k = 0$, which results from the requirement of momentum conservation. Also, the electromagnetic waves couple only to the transverse optical modes (because of the need for a dipole). Thus, although there is a continuous range of phonon energies in a crystal (for various k values), the IR spectrum consists of only a few discrete absorption peaks representing the number of optical vibrational modes at $k \approx 0$. It is to be noted that the presence of fewer absorption peaks in IR of a crystal is not due to the paucity of phonons of different energies but due to the condition of coupling with electromagnetic radiation which restricts it to optical phonons with $k \approx 0$. There is a Raman-IR complementarity in the spectra; totally symmetrical vibrational modes are Raman active and IR inactive (this complementarity is a result of mutual exclusion rule according to which a normal mode is not active in both Raman and IR spectra if the vibrational species has an inversion centre).

As we mentioned earlier, two distinct groups of vibrations can be identified in molecular crystals. The first category is the group of internal modes of the molecule which remain largely unaffected in the crystal. The second is the group of the external modes which like in the crystal discussed above exhibit the behaviour of lattice phonons. We may now consider the vibrational spectrum to be expected from a glass or an amorphous solid. Since there is no long range order, the small units of the structure which possess short range order, are connected to each other with no repetition. These small units may all be compositionally similar but may be considered as weakly coupled among themselves. Therefore the spectra will consist of features attributable to those units except that the inherent spread in bond angles, bond lengths and occasionally compositions would broaden the spectral features either due to a spread in the values of force constants or due to damping terms. If this were not the case, there would have been a continuous density of vibrational states with no momentum conservation rules to impose, and we would have observed a totally featureless IR spectrum contrary to experimental observations. The same conclusion can be arrived at by treating glass as a disordered crystal and relaxing the $k = 0$ absorption condition. However, the observed spectra can be consistent only when the IR coupling strength to a given mode is a strongly decreasing function of k.

Raman spectroscopy

The theory of Raman spectroscopy suggests that the scattering depends on electronic polarizabilities of the atoms and the dipole moments accompanying the changes in polarizabilities. Raman scattering is in principle a three step process (1) the change in polarizability causing a transition from the ground state to a virtual excited state (2) creation (or annihilation) of phonons by an electron-phonon interaction and (3) return to the electronic ground state. Thus the polarizability plays a key role in Raman spectroscopy. Both the polarizability, α, (which is a tensor) and the associated electric moment M (a vector) can be expanded in terms of normal mode displacements (which are vectors). Thus

$$\alpha = \alpha^{(0)} + \alpha^{(1)}x + \alpha^{(2)}x^2 + ... \tag{4.52}$$

where x is the normal mode displacement. The electric dipole moment M can now be written as

$$M = \alpha E = \alpha^{(0)}E_0 e^{i\omega t} + \alpha^{(1)}xE_0 e^{i(\omega \pm w_j)t} + \alpha^{(2)}x^2 E_0 e^{i(\omega \pm 2w_j)t} + ... \tag{4.53}$$

The above equation contains the origin of all the spectra we observe. The first term is a simple excitation-deexcitation process leading to the Rayleigh scattering. The second term involves the first derivative of polarizability and is responsible for creation and annihilation of phonons of frequency ω_j. When the phonons are due to low frequency acoustic modes, it corresponds to Brillouin scattering with an energy range of 0.1-1 cm^{-1}. When these phonons have energies in the infrared region, as high as 10^2-10^3 cm^{-1}, it corresponds to Raman scattering. It may involve both high energy acoustic and optical phonons. The term consisting of $\alpha^{(2)}$ in the above equation describes the multiphonon processes.

Thus the condition for observation of Raman spectrum is a non-zero $\alpha^{(1)}$, which is the selection rule. The intensity of Raman scattering, however depends on a number of factors, which includes the frequency of the scattered light (energy separation and hence populations), the density of vibrational states, the damping constant etc. In the case of glasses, an expression due to Shuker and Gammon (1971) for the Raman intensity of the Stokes lines is given by,

$$I(\omega) \approx \frac{1+n(\omega)}{\omega}\sum_b c_b g_b(\omega) \tag{4.54}$$

where b is the vibrational band index and $g_b(\omega)$ is the density of states, for the band b and c_b is the factor which depends on the correlation length associated with the modes in band b. Thus, the spectrum consists of the weighted sum of the densities of states of various bands. The explicit temperature dependence can be removed by dividing the measured intensities by $[1 + n(\omega)]$, which is the Bose-Einestein factor. The resulting spectrum is known as the reduced Raman spectrum. In the Raman spectra of glasses, a quantity known as Raman depolarization ratio is often reported and it is very useful in the interpretation of the spectra. The depolarization ratio ρ is given by,

$$\rho = \frac{I_{\parallel}}{I_{\perp}} \tag{4.55}$$

where $I_{\parallel}$ and $I_{\perp}$ are the Raman intensities measured with their plane of polarization parallel to and perpendicular to that of the incident beam respectively. Instead of stating parallel or perpendicular they are often subscripted as *HH*, *VV*, *VH* and *HV*, where *H* and *V* stand for horizontal and vertical polarization and their order being first for the incident and then for the scattered frequencies. The variation of the depolarization ratio for amorphous solids is somewhat similar to those of molecules. For a completely isotropic disordered solid, ρ lies between 0 and 3/4 and only the non-symmetric modes give a ρ value equal to 3/4. Thus, the depolarization ratio can be used as a factor in inferring the presence of symmetric modes of vibrations. The preceding discussion provides the necessary background for understanding the IR and Raman spectra to be discussed in subsequent chapters. Generally the glass spectra reveal the presence of frequencies attributable to chemical entities and together with other data related to the chemistry of the glass, fair amount of structural information can be obtained even using a 'fingerprint' identification process, which is why vibrational spectroscopy has been the most popular tool in the structural investigation of glasses.

X-ray Photoelectron Spectroscopy

X-ray photoelectron spectroscopy (XPS) and ultraviolet photoelectron spectroscopy (UVPES) are two techniques of great value in the study of the structure of glasses. In recent times, quantitative study of non-bridging oxygens in glasses, surface phenomena such as nitridation etc. have been studied (Stephenson and Binkowski, 1976; Nagel et al.,

1976; Fischer et al., 1977; Ching et al., 1985) using photoelectron spectroscopy (PES). The technique is based on the use of the well-known photoelectric effect. When X-ray or UV photons are incident on the surface of a glass (or any material), electrons are ejected from the material. This photoionization is governed by the relation,

$$h\nu = \phi + \frac{1}{2}m\mathrm{v}^2 \tag{4.56}$$

where ϕ is the binding energy and $(1/2)m\mathrm{v}^2$ is the kinetic energy of the photoelectron. The binding energies are the characteristic energies of the electrons in an atom and are therefore atom specific. When UV photons are used, the energies are sufficient to liberate electrons only from valence levels. But X-ray photons such as Al-Kα or Mg-Kα, which have energies of 1487 eV and 1254 eV respectively, used in XPS are capable of ionizing electrons from the core levels of atoms. The study of PES, therefore, consists of determining the kinetic energy of the ejected electrons, which through equation (4.56) determine the binding energy of the electrons for a fixed energy of irradiating photon. Thus in an atom, where electrons are present in various levels with different binding energies, PES consists of a series of peaks corresponding to the binding energies of various electrons. The electron binding energies decrease in the order 1*s*, 2*s*, 2*p*, 3*s*, 3*p*, 4*s*, 3*d*, 4*p* etc. levels. Further, due to Russell-Saunders coupling 2*p*, 3*p*, 3*d* etc. levels are split as $2p^{1/2}$, $2p^{3/2}$, $3p^{1/2}$, $3p^{3/2}$, $3d^{3/2}$, $3d^{5/2}$ etc. A few factors complicate the situation and render the equation (4.56) above, approximate. First is the assumption that the energy levels in the atom are frozen and therefore the ionisation process does not affect other energy states. But in practice, there is always a relaxation associated with photoionization, which therefore reduces the kinetic energy of the ionised electron. The second factor is that the released photoelectron has to cross a surface barrier, ϕ_a, before reaching the detector, which again reduces the kinetic energy of the photoelectron. During irradiation of an insulator, the surface of the sample gets charged due to both PES and Auger processes (see later) and emission of low energy secondary electrons. This build up of the positive charge also decreases the kinetic energy of the photoelectrons. A simple method of removing this last effect is to flood the surface of the sample with low energy electrons using an electron flood gun. The relaxation energy is however a characteristic of the atom and is independent of the composition and chemical structure. The binding energy value is therefore readily corrected. In the standard practice, the

binding energy is determined using a calibrant along with the material under investigation and the photoelectron binding energies of the calibrant are known. C 1*s* binding energy (= 285 eV) (Swift, 1982; Hohiki and Oki, 1984) is used almost universally. Since most specimen exposed to atmosphere, contain carbonaceous surface contamination, there is generally a C 1s peak of the adventitious carbon, which always provides a fortuitous calibration. In glasses, sometimes it is advantageous to have an internal standard of an element, which is a component of glass itself. It is further considered advantageous to refer the binding energy to the Fermi level rather to the vacuum level.

A secondary effect occurs in most photo-emission experiments and is known as Auger emission. Auger electron spectra is also a valuable experimental technique. When a core electron, say, from 1s level of an element is ionized, the hole created in the K shell leaves the atom in an excited state. The deexcitation of the atom occurs by the jumping of an outer shell electron into the K-shell vacancy, which now emits a X-ray photon corresponding to the energy difference of the two levels involved. This newly emitted X-ray photon (necessarily of lower energy) ionizes yet another electron, usually in the outer levels. This is the *Auger electron.* The process may involve, for example, an L electron jumping into the K shell and the energy released ionising another L electron. It is schematically shown in Figure 4.19. Thus the Auger process involves 3 levels – core level corresponding to the first photoionization (K), the level

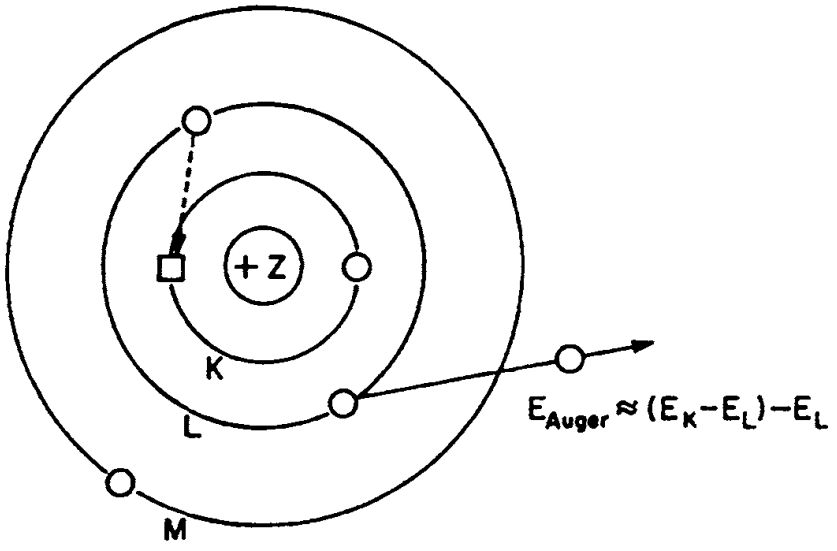

Figure 4.19: Orbital model of the electron transitions associated with de-excitation of a core-level vacancy by the Auger (KLL) emission process. The two L levels are the L_1 and L_2 in the text.

from which the electron jumped to fill the core level (L_1) and the level from which Auger electron was liberated (L_2). Since the levels involved are at fixed energies, the emitted electron has a characteristic kinetic energy. Therefore, the kinetic energy of Auger electron, designated as E_{KLL} is given by

$$E_{KLL} = E_K - E_{L1} - E_{L2} - \phi_a \tag{4.57}$$

where ϕ_a is the energy difference between vacuum and Fermi levels. These energies have been listed for various atoms. Auger emissions are particularly dominant for low Z atoms in the photo electron spectrum. In the literature, a quantity known as Auger parameter, is often measured. This is the difference in the kinetic energies of any chosen photoelectron and that of an Auger electron. These are generally constant for a given element and useful in the identification of that element in compositional analysis.

The most valuable application of XPS is in the determination of the chemical state of a given element through the measurement of the chemical shift. Chemical shift is the alteration of binding energy caused by the nature of the chemical environment and bonding characteristics of an element to its neighbours, Thus, for example, Si 2*p* binding energy varies by as much as 7 eV in its compounds as shown in Table 4.3. This variation in binding energy can also be very low (a fraction of an eV) as in the case of O 1*s* levels for the bridging and non-bridging varieties. Measurements of such differences require a very high resolution photoelectron spectrometer.

Table 4.3: Variation of Si 2*p* binding energy in different compounds (After Castle and West, 1980).

Sample	Formula	Si 2p BE (eV)
Silicon	Si	99.6
Silicon carbide	SiC	103.9
Silicon nitride	Si_3N_4	102.0
Silicon dioxide	SiO_2	102.6
Zinc silicate	$ZnSiO_3$	108.1
Silica gel	$SiO_2.xH_2O$	107.0

Both PES and Auger spectroscopies are considered as surface techniques. It is because the ejected photo electron has to escape from the surface with its true kinetic energy in order that the measurement is accurate. Electron should not suffer any inelastic scattering before its escape. Therefore, there is a characteristic depth parameter or the permissible escape depth, λ, which is also known as inelastic mean free path. It is the depth from below which the liberated electron has less than 63 % chance of escape without experiencing an inelastic scattering event. About 95 % of the detected signal in XPS originates from sampling depths of about 3λ. λ is of course a function of electron kinetic energy and in the range of 100 – 1000 eV. λ is of the order of 5 – 50 Å in oxides but it is much less for metals.

XPS has been used very successfully for the investigation of modification in oxide glasses. A typical example is shown in Figure 4.20.

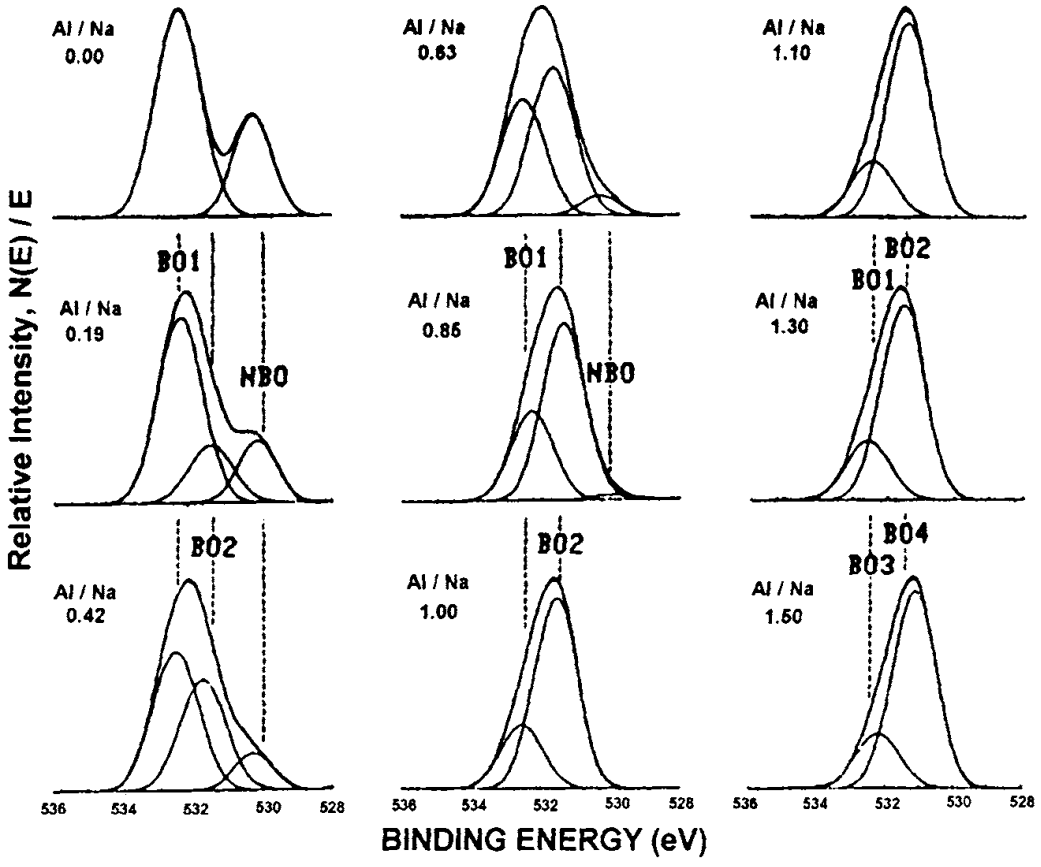

Figure 4.20: High-resolution O 1s spectra of sodium-aluminosilicate glasses with various Al/Na concentration ratios; each spectra was deconvoluted assuming three Gaussian components of constant width but varying binding energy (After Tusker et al., 1985).

The most important observation in the spectra of Figure 4.20 is the reduction of NBO when Al/Na ratio increases systematically.

In principle all of the techniques used for the investigation of crystalline solids are equally useful in the investigation of glasses. Several such characterization techniques are described briefly in other chapters where they are of immediate relevance. The effort in this chapter has been to put together the most important structural techniques used in glass science.

References:

Andrew, E.R., A. Bradbury and R.G. Eades, 1959, Nature, **183**, 1802.

Balkanski, M., 1971, Light scattering in Solids (Flammarion Sciences, Paris).

Bendow, B., 1993, in Experimental Techniques in Glass Science, eds. C.J. Simmons and O.H. El-Bayoumi (The American Ceramic Society, Ohio) p. 33.

Bursukova, M.A., E.A. Kashchieva and Y.B. Dimitriev, 1995, J. Non-Cryst. Sol., **192&193**, 40.

Castle, J.E., and R.H. West, 1980, J. Elect. Spec., **18**, 355.

Ching, W.Y., Y.P. Li, B.W. Veal and D.J. Lam, 1985, Phys. Rev. B., **32**, 1203.

Cummins, H. in Light scattering in Solids ed. M. Balkanski, 1971, (Flammarion Sciences, Paris) p. 3.

Elliott, S.R., 1978, Philos. Mag. B., **37**, 435.

Elliott, S.R., 1984, Physics of Amorphous Materials (Longman, London).

Emerson, J.F., and P.J. Bray, 1993, in Experimental Techniques in Glass Science, eds. C.J. Simmons and O.H. El-Bayoumi (The American Ceramic Society, Ohio) p. 77.

Fadini, A., and F.M. Schneppel, 1989, Vibrational Spectroscopy Methods and

Applications (Ellis Horwood Ltd., Chichester).

Farrar, T.C., and E.D. Becker, 1971, Pulse and Fourier Transform NMR: Introduction to Theory and Methods (Academic Press, New York).

Fischer, B., R.A. Pollak, T.H. DiStefano and W.D. Grobman, 1977, Phys. Rev. B., **15**, 3193.

Fukishima, E., and S.B.W. Roeder, 1981, Experimental Pulsed NMR, A Nuts and Bolts Approach (Addison-Wesley, Reading, Massachusettes).

Fyfe, C.A., 1983, Solid State NMR for Chemists (C.N.S. Press, Guelph).

Gurmann, S. and R.F. Pettifier, 1979, Philos. Mag. B., **40** 345.

Hahn, E.L., 1950, Phys. Rev. Lett., **80**, 580.

Hendrickson, J.R., and P.J. Bray, 1973, J. Mag. Reson., **9**, 341.

Hohiki, S., and K. Oki, 1984, J. Electron Spectrosc. Relat. Phenom., **33**, 375.

Lamparter, P., W. Sperl, E. Nold, G. Rainer-Harbach and S. Steeb, 1982, Proc. 4th Int. Conf. On Rapidly Quenched Metals, eds. Masumoto and J. Suzuki, (Jpn. Inst. Of Metals), p. 343.

Leadbetter, A.J., 1973, in Chemical Applications of Thermal Neutron Scattering, ed. B.T.M. Wills (OUP) p. 146.

Lerner, J.M., and F. Adar, 1989, Laser Focus World, **25**, 73.

Lewis, M.H., 1989, Glasses and Glass Ceramics (Chapman and Hall, New York).

Long, D.A., 1977, Raman Spectroscopy (McGraw-Hill, New York).

Lorch, E., 1969, J. Phys. C., **2**, 229.

Loudon, R., 1964, Adv. Phys., **13**, 423.

Lowe, I.J., 1959, Phys. Rev. Lett., **2**, 285.

Mehring, M., 1978, High Resolution NMR Spectroscopy in Solids (Springer-Verlag, Heisenberg).

Mitra, S.S., 1969, Opical Properties of Solids (Plenum Press, New York) p. 333.

Nagel, S.R., J. Tauc and B.G. Bagley, 1976, Solid State Comm., **20**, 245.

Prabakar, S., K.J. Rao and C.N.R. Rao, 1990, Proc. Royal Soc. (London), **A429**, 1.

Price, D.L., and J.M. Carpenter, 1987, J. Non-Cryst. Sol., **92**, 153.

Rao, C.N.R., 1963, Chemical Applications of Infrared Spectroscopy (Academic Press, New York).

Rao, K.J., J. Wong and M.J. Weber, 1983, J. Chem. Phys., **78**, 6228.

Sathyanarayana, D.N., 1996, Vibrational Spectroscopy: Theory and Applications (New Age Int. Publishers, New Delhi).

Sayers, D.E., E.A. Stern and F.W Lytle, 1971, Phys. Rev. Lett., **27**, 1204.

Shuker, R., and R. Gammon, 1971, Light scattering in Solids (Flammarion Sciences, Paris) p. 334.

Sinclair, R.N., 1985, J. Non-Cryst. Sol., **76**, 61.

Stephenson, D.A., and N.J. Binkowski, 1976, J. Non-Cryst. Sol., **22**, 399.

Swift, P., 1982, Surf. Interface Anal., **4**, 47.

Tusker, G.W., D.R. Uhlmann, P.I.K. Onorato, M.N. Alexander and C.W. Struck, 1985, J. de Physique, **C8**, C8-273.

Van Vleck, J.H., 1948, Phys. Rev., **74**, 1168.

Wagner, C.N.J., 1978, J. Non-Cryst. Sol., **31**, 1.

Warren, B.E., 1969, X-ray Diffraction (Addison-Wesley).

Waugh, J.S., L.M. Huber and U. Haeberlen, 1968, Phys. Rev. Lett., **20**, 180.

Wong, J., and C.A. Angell, 1976, Glass Structure and Spectroscopy (Marcel Dekker, Inc., New York).

Wright, A.C., 1993, in Experimental Techniques in Glass Science, eds. C.J. Simmons and O.H. El-Bayoumi (The American Ceramic Society, Ohio) p. 205.

Wright, A.C., 1974, Adv. Struct. Res. Diffr. Meth., **5**, 1.

Wright, A.C., and A.J. Leadbetter, 1976, Phys. Chem. Glasses, **17**, 122.

Wright, A.C., 1980, J. Non-Cryst. Sol., **40**, 325.

Zarzycki, J., 1982, Les Verres et L'état Vitreaux (Masson, Paris).